
Theses and Dissertations

Summer 2010

A biomechanical model of femoral forces during functional electrical stimulation after spinal cord injury in supine and seated positions

Colleen Louise McHenry
University of Iowa

Copyright 2010 Colleen Louise McHenry

This thesis is available at Iowa Research Online: <http://ir.uiowa.edu/etd/710>

Recommended Citation

McHenry, Colleen Louise. "A biomechanical model of femoral forces during functional electrical stimulation after spinal cord injury in supine and seated positions." MS (Master of Science) thesis, University of Iowa, 2010.
<http://ir.uiowa.edu/etd/710>.

Follow this and additional works at: <http://ir.uiowa.edu/etd>



Part of the [Biomedical Engineering and Bioengineering Commons](#)

A BIOMECHANICAL MODEL OF FEMORAL FORCES DURING
FUNCTIONAL ELECTRICAL STIMULATION AFTER SPINAL
CORD INJURY IN SUPINE AND SEATED POSITIONS

by

Colleen Louise McHenry

A thesis submitted in partial fulfillment
of the requirements for the Master of
Science degree in Biomedical Engineering
in the Graduate College of
The University of Iowa

July 2010

Thesis Supervisors: Professor Richard K. Shields
Associate Professor Nicole M. Grosland

Copyright by
COLLEEN LOUISE MCHENRY
2010
All Rights Reserved

Graduate College
The University of Iowa
Iowa City, Iowa

CERTIFICATE OF APPROVAL

MASTER'S THESIS

This is to certify that the Master's thesis of

Colleen Louise McHenry

has been approved by the Examining Committee
for the thesis requirement for the Master of Science degree in Biomedical
Engineering at the July 2010 graduation.

Thesis Committee: _____
Nicole M. Grosland, Thesis Supervisor

Richard K. Shields, Thesis Supervisor

Tae-Hong Lim

ACKNOWLEDGMENTS

First, I would like to thank the Neuromuscular Lab in the Physical Therapy and Rehabilitation Science department. I not only completed my master's thesis in their lab, but also was inspired to continue my education in this department. My advisor, Dr. Richard Shields, has guided me throughout this project and has prompted questions which encouraged independent thought. My lab mates, Andy and Shauna, have mentored me and offered their expertise throughout the project. Shauna has been there to critically examine my rationale and my findings which led me to build stronger arguments and not settle with the first attempt. I also want to thank the Biomedical Engineering department for teaching me the critical thinking and problem solving skills required to complete my master's thesis especially my academic advisor, Dr. Nicole Grosland.

I also need to recognize and thank those who have personally supported me throughout this process. My parents, Mark and Michelle McHenry, fostered an environment conducive to learning and academic success. They promoted analytical thinking and creativity in a loving, warm home. My sisters, Molly and Emily, and my brother, Jonathan, have been there to offer words of encouragement and to make me laugh. I would also like to thank the many friends that have supported me during this process, especially Mike for giving his time and troubleshooting skills. Finally, I would like to thank my friend and roommate, Cassie, for always listening and motivating me to complete this project. Throughout these two years, she has been there to offer a warm meal and much needed words of encouragement. I would not have been able to finish this project without all of these wonderful individuals.

ABSTRACT

Following a spinal cord injury (SCI), the paralyzed extremities undergo muscle atrophy and decrease in bone mineral density (BMD) due in part to the loss of physiological loading. It is crucial to prevent musculoskeletal deterioration so the population is less susceptible to fractures, and could take advantage of stem cell treatment if it becomes available. Functional electrical stimulation (FES) has been shown to advantageously train the paralyzed extremities. However, there is a risk of fracture during FES due to low BMD of individuals with SCI. Therefore, the forces generated during FES need to be modeled so researchers and clinicians safely administer this intervention.

The purpose of this project was to develop a biomechanical or mathematical model to estimate the internal compressive and shear forces at the distal femur, a common fracture site for individuals with SCI during FES. Therefore, a two-dimensional static model was created of the lower extremity in the supine and seated positions. The compressive and shear forces at the distal femur were estimated for both positions during FES. These internal compressive and shear forces estimated at the distal femur by the supine model were compared to those estimated by the standing model. Also, for the seated model, the compressive and shear forces at the distal femur estimated by a tetanic muscle contraction were compared to those estimated by a doublet muscle contraction. Finally, the supine model was validated using experimental testing.

The primary findings are 1) the standing model estimated more compressive force and less shear force at the distal femur compared to the supine model when position and quadriceps muscle force remain constant and 2) for the seated model, a tetanic quadriceps muscle contraction predicts greater compressive and shear at the distal femur compared to a doublet muscle contraction. Also the validation testing revealed a 3.4% error between the supine model and the experimental testing. These models provide valuable insights into the internal forces at the distal femur during FES for those with SCI.

TABLE OF CONTENTS

LIST OF TABLES	vi
LIST OF FIGURES	vii
CHAPTER 1 INTRODUCTION	1
Background.....	1
Purpose and Specific Aims	1
Hypothesis	3
CHAPTER 2 LITERATURE REVIEW	4
Muscle and Nerve Anatomy	4
Musculoskeletal Adaptations Following SCI	4
Methods and Implications of Training Individuals with SCI	5
Rationale for Creating a Biomechanical Model	7
CHAPTER 3 METHODS	14
Mathematical Model.....	14
Supine Model.....	14
Supine Static Equilibrium Equations.....	15
Supine Compression and Shear Equations	16
Seated Model	16
Seated Static Equilibrium Equations	17
Seated Compression and Shear Equations	17
Experimental Testing Conditions	18
Supine Model.....	18
Seated Model	19
Data Collection and Analysis	20
CHAPTER 4 RESULTS	29
Experimental Results.....	29
Mathematical Model Predictions.....	29
Supine Model Predictions.....	29
Supine and Standing Model Comparisons	30
Seated Model Predictions	31
Validity of Mathematical Models.....	32
CHAPTER 5 DISCUSSION.....	46
Limitations and Future Work.....	48
Conclusions.....	49
REFERENCES	51
APPENDIX A MODEL PARAMETERS	57
APPENDIX B MATLAB CODE FOR THE SUPINE MODEL.....	58

APPENDIX C MATLAB CODE FOR THE SEATED MODEL	61
---------------------------------------------------	----

LIST OF TABLES

Table

1. The six supine positions with the corresponding thigh angle(φ) and shank angle (α)21
2. The solution to the five unknowns of the seated model for tetanic and doublet pulses are quadriceps force (F_{quad}), the horizontal force at the hip (F_{xhip}), the vertical force at the hip (F_{yhip}), compressive force at the distal femur (F_c), and shear force at the distal femur (F_v) and are reported in terms of percent body weight.....45

FIGURES

Figure

1.	Schematic free body diagram of the lower body during (A) passive stance and (B) active (no added resistance, $R=0$) and/or active-resistive stance ($R = 16.7\text{-}67.7\% \text{ BW}$). The internal forces from the quadriceps and patellar tendons (F_{quad} and F_{pat} , respectively) in B) replace the F_{pad} in (A)	10
2.	Modeled quadriceps forces are shown in percent body weight (% BW) during active and active-resistive stance with resistances ranging from 16.7% BW to 67.7% BW for each of the six stance postures	11
3.	Modeled distal femur compression (A) and shear (B) in terms of percent body weight are plotted for passive, active, and active-resistive stance at each of the six stance postures. Note the different scales between graph A and B.	12
4.	Schematic representations of six possible stance postures for individuals with spinal cord injury (SCI) using an external frame (not shown). The arrow at the hip and the vertical line at the knee represent a hip support belt and a knee support pad, respectively. The feet are placed on the ground.....	13
5.	Schematic free body diagram of the external forces and loading conditions acting on the lower extremity for the supine model	21
6.	Schematic representation of the relationship between the quadriceps tendon or muscle (F_{quad}) and the patellar tendon (F_{pat}) at the knee joint.	22
7.	Schematic free body diagram of the distal femur for the supine model which has been cut at 85% of thigh segment length from the hip joint. The bending moment at the distal femur was not determined but the compressive force (F_c) and shear force (F_v) were calculated.	23
8.	Schematic free body diagram of the external forces and loading conditions acting on the lower extremity for the seated model.....	24
9.	Schematic free body diagram of the distal femur for the seated model which has been cut at 85% of thigh segment length from the hip joint. The bending moment at the distal femur was not determined but the compressive force (F_c) and shear force (F_v) were calculated.	25
10.	Placement of surface electrodes over the quadriceps muscle	26
11.	Non-SCI male positioned on the KinCom for the experimental supine model.....	27
12.	Schematic of the experimental seated model of the doublet stimulation protocol	28
13.	The supine model predictions for the forces at the tibial restraint, R_A , at various quadriceps muscle forces for the six different supine positions are graphed in terms of percent body weight (%BW).	33

14.	The estimates of the horizontal forces at the hip, F_{xhip} , for the supine model at various quadriceps muscle forces for the six different supine positions are plotted in terms of percent body weight (%BW).....	34
15.	The supine model estimates of the horizontal forces at the hip, F_{yhip} , are plotted in terms of percent body weight (%BW) for the six supine position with five different quadriceps muscle forces at each position.....	35
16.	The compressive forces, F_c , estimated at the distal femur for the supine model in percent body weight (%BW) and graphed against quadriceps force.....	36
17.	The shear forces, F_v , estimated at the distal femur for the supine model in percent body weight (%BW) and graphed against quadriceps force.....	37
18.	The estimates from the supine model for the tibial restraint force, the horizontal and vertical forces at the hip, and the compressive and shear forces at the distal femur for position 1 at five quadriceps forces.....	38
19.	The compressive forces at the distal femur for the supine model and the standing model are plotted in terms of body weight (%BW) with respect to quadriceps muscle force.....	39
20.	Compressive forces at the distal femur of the supine and standing models separated by position and plotted in terms of percent body weight (%BW)	40
21.	A representative example of the compressive forces at the distal femur of position 1 for the supine and standing models as a percent of body weight (%BW) plotted against quadriceps muscle force.....	41
22.	The shear forces at the distal femur for both models, supine and standing, are plotted in terms of percent body weight (%BW) as a function of quadriceps muscle force.....	42
23.	Shear forces at the distal femur of the supine and standing model separated by position and plotted in terms of percent body weight (%BW)..	43
24.	A representative example of the shear forces at position 1 for the supine and standing model as a percent of body weight (%BW) plotted against quadriceps muscle force.....	44

CHAPTER 1 INTRODUCTION

Background

Spinal cord injury (SCI) affects 11,000 individuals a year in the U.S. and has many physical, emotional, and psychological repercussions for these individuals and their families [1]. Spinal cord injury occurs when there is a lesion to the spinal cord that results in a loss of sensorimotor function [2]. Individuals with SCI can be classified as having a complete injury with no motor or sensory function, or an incomplete injury where some sensation is intact and possibly some motor function remains [3]. Regardless of the SCI classification, those with SCI are twice as likely to have lower extremity fractures than the general population [4] due to musculoskeletal deterioration and experience a variety of secondary complications such as deep vein thrombosis, pressure ulcers, and urinary tract infections. Typically, they have a decrease in the health-rated quality of life compared to age and gender matched controls [5]. However, exercise or “training” protocols could offer some benefits to individuals with SCI and counteract some of the adverse effects of this injury. With the advent of stem cell research, we are hopefully approaching a cure or treatment program for those suffering from SCI. However, if the integrity of the paralyzed extremities has been severely compromised, then these individuals will be unable to take advantage of such a medical breakthrough.

Purpose and Specific Aims

Since individuals with SCI cannot naturally load their lower extremities through volitional movement or exercise, other methods of activation must be used such as functional electrical stimulation (FES). FES uses an electrical current to activate the peripheral nerve and thereby the muscle it innervates and in most cases is a viable option to train the paralyzed extremities. It can be coupled with other methods of training like cycling or standing. Also, the frequency of the FES determines the type of muscle contraction. If there is only one electrical pulse then a muscle twitch will result. However, if a second electrical

pulse is delivered before the muscle can relax (~100 ms) then summation of the force occurs [6]. A doublet occurs when two muscle impulses are delivered, and depending on the frequency of the electrical pulses, summation can occur. If the frequency is high, such as 30 Hz, then force summation should occur, but if it is low, such as 5 Hz, then the force will not summate. Twitches and doublets are safe, effective ways to determine muscle physiology; however, training muscle involves a different kind of muscle contraction known as a tetanic train. Tetanic trains or contractions occur when many electrical pulses are delivered to the muscle at a high frequency. When training muscle of SCI individuals, tetanic contractions are used to emulate volitional muscle contractions.

During training protocols for SCI individuals, it is impossible to accurately measure the forces acting on the bone in vivo. Osteoporosis develops rapidly after SCI [7, 8], and large muscle forces could cause fractures in bones with poor density or architecture. Therefore, these forces need to be modeled in a way that will make it easier for clinicians and researchers to safely provide an intervention to the vulnerable SCI population. A biomechanical model or a mathematical model is one way to predict the forces that would be generated by the muscle, and therefore, the forces experienced by the bone. The purpose of this study was to create a mathematical model which estimates the compressive and shear forces at the distal femur, a common fracture site for SCI individuals [9]. The model will contrast a previously developed model of standing with two positions not previously modeled for SCI: seated and supine. The seated position is often used during functional electrical stimulation (FES) training because the patient can remain in his/her wheelchair and the quadriceps muscle is at its optimal length [10, 11]. The supine position was chosen so that it can be easily compared to a previously developed standing model. Currently, there are no models to estimate the loads during FES for these two positions. Therefore, the specific aims of this study are:

1. To create static two-dimensional, mathematical models of the lower extremity while

the subject is a) supine and b) seated.

2. To estimate the loading environment of the distal femur during functional electrical stimulation training for those with SCI in the seated and supine positions.
3. To compare shear and compressive forces generated at the distal femur in the supine model to the standing model
4. To compare shear and compressive forces at the distal femur of the seated model during a tetanic quadriceps muscle contraction and during a doublet quadriceps muscle contraction.
5. To validate the supine model by comparing the predicted force at the tibial restraint with the force measured during the experimental testing.

Hypothesis

The general hypothesis is that the standing model is superior to the alternative positions (supine, seated) in terms of optimal compressive loads and minimizing dangerous shear forces on the distal femur. The specific hypotheses are as follows:

Hypothesis 1: If the quadriceps force from the standing model and the supine model remain the same and the angles of the lower limb are held constant, the compressive forces will be significantly lower and the shear forces will be significantly higher in the supine model.

Hypothesis 2: For the seated model, a doublet pulse will result in significantly lower shear and compressive forces at the distal femur compared to a tetanic train.

CHAPTER 2 LITERATURE REVIEW

Muscle and Nerve Anatomy

The spinal cord is part of the central nervous system. It serves to transmit motor commands from the brain to the periphery, and carries sensory information from the periphery to the brain. The spinal cord originates at the brainstem, travels through the foramen magnum in the base of the skull, and continues within the vertebral column branching off and becoming peripheral nerves. These peripheral nerves are composed of many axons; each axon branches further until it innervates a single muscle fiber.

Voluntary or volitional muscle contractions occur when an electrical signal travels from the brain to the muscle via the spinal cord and its peripheral nerves. If these conduits for electrical signals are damaged then the brain can no longer send commands to the muscle or receive feedback from the muscle. A spinal cord injury is an example of such a disturbance to the nervous system and can result in a loss of volitional movement. Typically, a SCI causes an upper motor neuron lesion as well as a lower motor neuron lesion. An upper motor neuron lesion is a disruption of upper motor neuron pathways descending to muscles and ascending sensory pathways from muscles, and a lower motor neuron lesion results in damage to peripheral nerves at the level of the injury.

Musculoskeletal Adaptations Following SCI

Spinal cord injury (SCI) results in muscle atrophy [12] and a rapid decrease in bone mineral density (BMD) of the paralyzed lower extremities due in part to the absence of physiological loading [13]. Muscle contractions naturally load the skeletal system and maintain BMD, but following a SCI this stimulus is removed. It has been observed that six weeks after a SCI, lower extremity muscles experience a 45% decrease in cross-sectional area compared to age-matched controls [14]. Also, there is a shift in fiber type to fast muscle [15, 16]. Normally, human muscle contains a combination of fast and slow muscle but following a SCI slow muscle transforms to fast muscle because it is more metabolically

efficient. Slow muscle, which is fatigue resistant, requires more oxygen, therefore, needs more blood vessels and more surface area to accommodate them [11]. The muscle transformation is reflected by an increase in myofibrillar adenosine triphosphatase (mATPase) [17].

Spinal cord injury severely restricts gravitational and muscle stimuli on the paralyzed extremities which are essential to maintaining bone density. When the bone is no longer mechanically loaded the osteoclast activity outpaces the osteoblast activity resulting in a decrease in bone mineral density and an alteration in bone microarchitecture. During the first year following SCI, the BMD of cortical bone decrease 2% per month and trabecular bone decreases 4% per month in the paralyzed extremities [18]. In a SCI femur, there is a 50% loss of trabecular bone in the epiphyses and a 35% decrease in cortical wall thickness of the shaft [8]. After a SCI, the trabecular lattice continues to be replaced with marrow [19] and a steady-state BMD is reached between 3 and 8 years post-injury [8]. The steady state BMD of SCI individuals is 50-60% less than those of non-SCI [20] which emphasizes the importance in preventing such deterioration.

Methods and Implications of Training Individuals with SCI

Many methods have been developed attempting to prevent muscle atrophy and osteoporosis in individuals with SCI including functional electrical stimulation (FES), FES cycling, body weight supported treadmill training, and standing. The purpose of exercise is to optimally stress muscle and bone in order to induce an advantageous adaptation and avoid injury [21]. In general, muscle hypertrophy occurs if a muscle experiences a certain amount of overload [20]. When a muscle experiences a large load through volitional activation or elicited by electrical stimulation it will adapt and increase its force generating capabilities. Bone has a similar response to training and to induce osteogenesis, bone formation, it needs to experience a certain amount of mechanical load [22]. Osteocytes, bone cells, are very sensitive to mechanical deformation or strain which results from fluid flow within the bone

and leads to bone adaptation [23]. According to Frost, bone modeling or formation occurs at 1500-3000 microstrain and bone remodeling or degradation occurs at 100-300 microstrain [24]. Therefore, bone needs to have a certain amount of strain in order to prevent degradation and osteoporosis. Following a SCI, it is crucial that muscle and bone are optimally loaded so that they do not deteriorate. While there are many methods to train the paralyzed musculoskeletal system of those with SCI; our lab has found that FES and FES coupled with standing can radically alter musculoskeletal physiology, especially compared to other training protocols.

Functional electrical stimulation (FES) uses a nerve to activate a muscle by an electrical current. It has been effective in activating paralyzed muscles to attenuate BMD loss [25, 26] and to prevent muscle atrophy after SCI [27]. FES can be used if there are no lower motor neuron lesions which would prevent electrical activation of the target muscle. Typically, if the muscle experiences adequate stimuli to induce muscle changes, then FES results an increase in muscle cross sectional area [28, 29], an increase in oxidative capacity [30, 31], and retention of slow muscle fiber [32]. For example, when stimulating wrist extensors in tetraplegics, the group that received higher stimulation, and therefore, a higher resistance force experienced an increase muscle strength compared to the low resistance group [33]. Also, a quadriceps study showed a correlation between the magnitude of load and the degree of muscle adaptation. The limb that received the higher load had a significant increase in cross-sectional area, Type I fibers, and a capillary-to-fiber ratio compared to the opposite limb [34]. Since muscle can retain its force generating capabilities through FES, they can provide a substantial mechanical load and affect bone mineral density. In previous work from our laboratory, unilateral FES of one soleus muscle resulted in a 31% increase in BMD of the tibia compared to the tibia of the untrained limb the same individual [35, 36]. The BMD of the posterior region of the tibia also remained close to the BMD of non-SCI individuals because the soleus stresses the tibia posteriorly [37]. It is essential to examine the magnitude of bone loading required to induce bone remodeling.

Osteogenesis occurs when bone reaches a strain level of 1500-3000 microstrain [24]. However, with spinal cord injury individuals it can be difficult to safely deliver a significant load to the lower extremities, because their atrophied muscles have reduced force generating abilities and their osteoporotic bones are susceptible to fractures. Passive standing using a standing frame or standing wheelchair is one way for individuals with SCI to mechanically load their lower extremities. Generally, passive standing does not affect BMD [38, 39] because the compressive load to the lower extremities is only 40% of body weight, as estimated by the previous standing model [40]. The soleus study showed that a load of approximately 150% of body weight was sufficient to cause an increase in BMD [35]. To incorporate FES and standing, a standing exercise paradigm has recently been developed to optimally load bone [40]. A 2-D model was created to examine the differences between passive standing, active standing where the quadriceps are activated enough to support body weight and active-resistive stance, where the quadriceps are activated enough to support body weight and push against an external resistance. As hypothesized, active-resistance stance produced the greatest amount of compressive force at the distal femur of 240% body weight but shear force was less than 24% body weight [40]. Through this experimental model the lower extremities can be optimally loaded while minimizing fracture-inducing shear stress.

Rationale for Creating a Biomechanical Model

Although FES is an ideal stimulus to trigger adaptations in paralyzed muscle and bone, those administering such interventions need to be aware of the potentially dangerous repercussions. Those with spinal cord injury are twice as likely as the general population to have a fracture [4] from routine activities. There is one published report of a bone fracture of a SCI subject during FES. The authors attributed the lateral femoral condyle fracture to maximal electrical stimulation while the knee was locked in 90° of flexion, muscle spasm during the stimulation, severe osteoporosis, and an increase in muscle strength from regular

bouts of FES cycling [41]. Therefore, it is important to account for the change in bone structure and to load the lower extremity in a safe way, in order to prevent such occurrences.

When administering FES training to a SCI cohort, it is crucial to understand the shear and compressive forces that are generated. It is believed that the documented fracture during FES was the result of a large shear force. In a biomechanical analysis of the knee, Smidt demonstrated that a change in the knee angle corresponded to a change in the magnitude and direction of the shear forces at the distal femur. The maximum posterior shear force (tibia moving posteriorly on the femur) occurs when the knee is in 90° of flexion [42], the same knee angle of the reported fracture. Clinicians and researchers use FES with the knee flexed to 90° because when a subject is seated and the knee is flexed at $90\text{-}100^\circ$ the quadriceps muscle is at its optimal length, therefore can generate its maximum torque [43]. The quadriceps muscle can generate such a large torque because in this position the patella and the femur have the greatest amount of contact [44-46]. Since the goal of FES is to prevent muscle atrophy and attenuate bone loss, those training want to safely deliver the highest dose possible to induce positive musculoskeletal adaptations.

One way to ensure safe training is to understand the forces that can be generated during a specific loading environment and position. Since it is difficult to directly measure the various forces on the bone in vivo, a model needs to be created to simulate the loading conditions during FES. A two-dimensional, mathematical model can provide valuable insight into the forces generated from certain loading conditions. Due to the simplicity of this model, it is easy to use for clinicians and researchers and provides a cost effective alternative to other models which require imaging. As stated earlier, a 2D, mathematical model has been created to investigate the external forces, quadriceps muscle forces, and the shear and compressive forces at the distal femur during FES while standing [40]. Figure 1 shows the free body diagram of the passive and active conditions used to determine the quadriceps muscle force (Fig. 2) and subsequently the compressive and shear force at the distal femur (Fig. 3). A range of resistive force, R , in terms of body weight were implemented in the

active condition model including 0%, 16.7%, 33.3%, 50%, and 67.7%. Figure 2 depicts the quadriceps muscle force as the resistive force and the stance position change. Six standing positions were used, resulting in different thigh and shank angles (Fig. 4). The greatest quadriceps force, 190% of body weight, occurs at position 6, the most upright posture, with a resistive force equivalent to 67.7% of body weight. While the largest compressive force is also produced during that position and resistive force, 240% of body weight, shear force remains relatively low at 24% of body weight. The standing model demonstrates that a large compressive force could be applied to the distal femur during this standing exercise paradigm while minimizing harmful shear forces.

One of the goals of this study is to develop a mathematical model for the supine position to compare the compressive and shear forces at the distal femur to those generated in the standing model. Another goal of the study is to create a seated mathematical model and estimate the shear and compressive forces at the distal femur during two different loading conditions. The first loading condition is a tetanic contraction which is elicited from the quadriceps muscle; more specifically, the force that was previously reported to cause a fracture (206 N) will be used. The second loading condition is the muscle contraction resulting from a doublet pulse delivered to the quadriceps muscle [43]. The doublet protocol was developed as a way to accurately measure muscle physiology without generating dangerously high forces. However, the shear and compressive forces at the distal femur during the doublet protocol have not been examined.

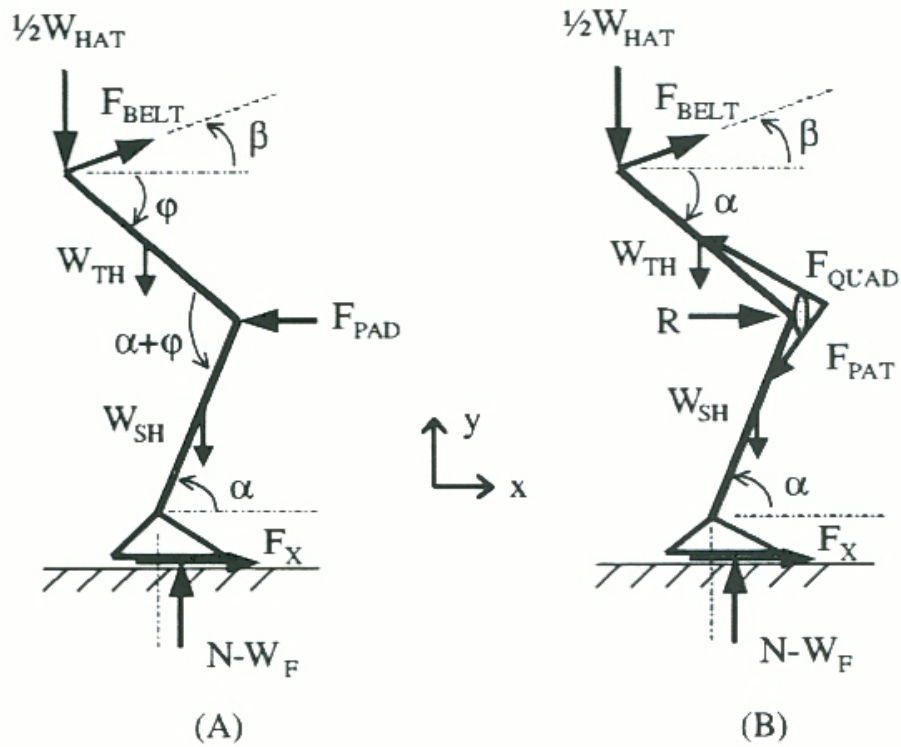


Figure 1. Schematic free body diagram of the lower body during (A) passive stance and (B) active (no added resistance, $R = 0$) and/or active-resistive stance ($R = 16.7\text{--}67.7\%$ BW). The internal forces from the quadriceps and patellar tendons (F_{quad} and F_{pat} , respectively) in (B) replace the F_{pad} in (A).

Source: Frey Law, L.A. and R.K. Shields, *Femoral loads during passive, active, and active-resistive stance after spinal cord injury: a mathematical model*. Clin Biomech (Bristol, Avon), 2004. **19**(3): p. 313-21.

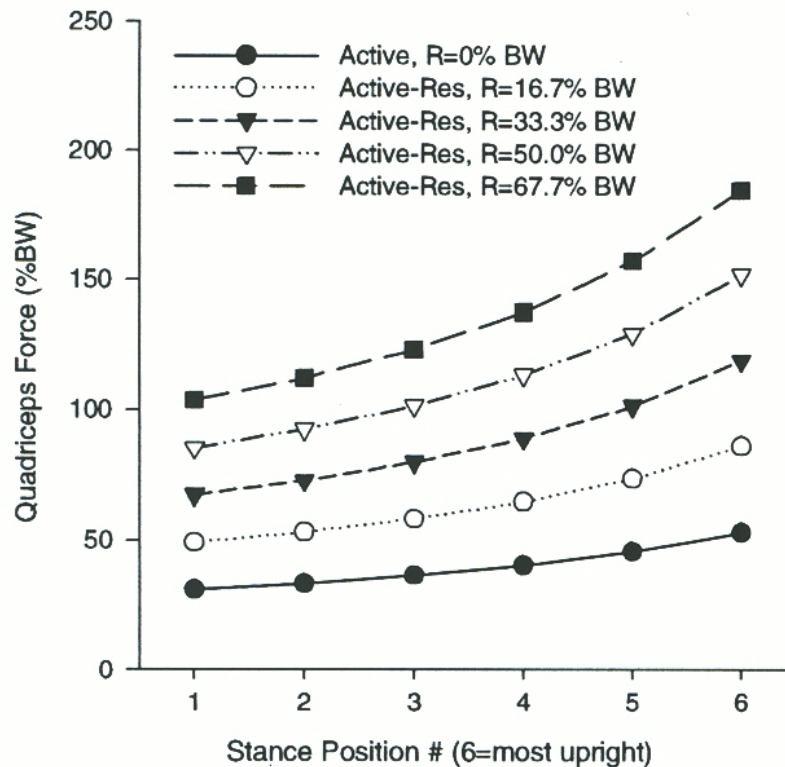


Figure 2. Modeled quadriceps forces are shown in percent body weight (% BW) during active and active-resistive stance with resistances ranging from 16.7% BW to 67.7% BW for each of the six stance postures.

Source: Frey Law, L.A. and R.K. Shields, Femoral loads during passive, active, and active-resistive stance after spinal cord injury: a mathematical model. Clin Biomech (Bristol, Avon), 2004. **19**(3): p. 313-21.

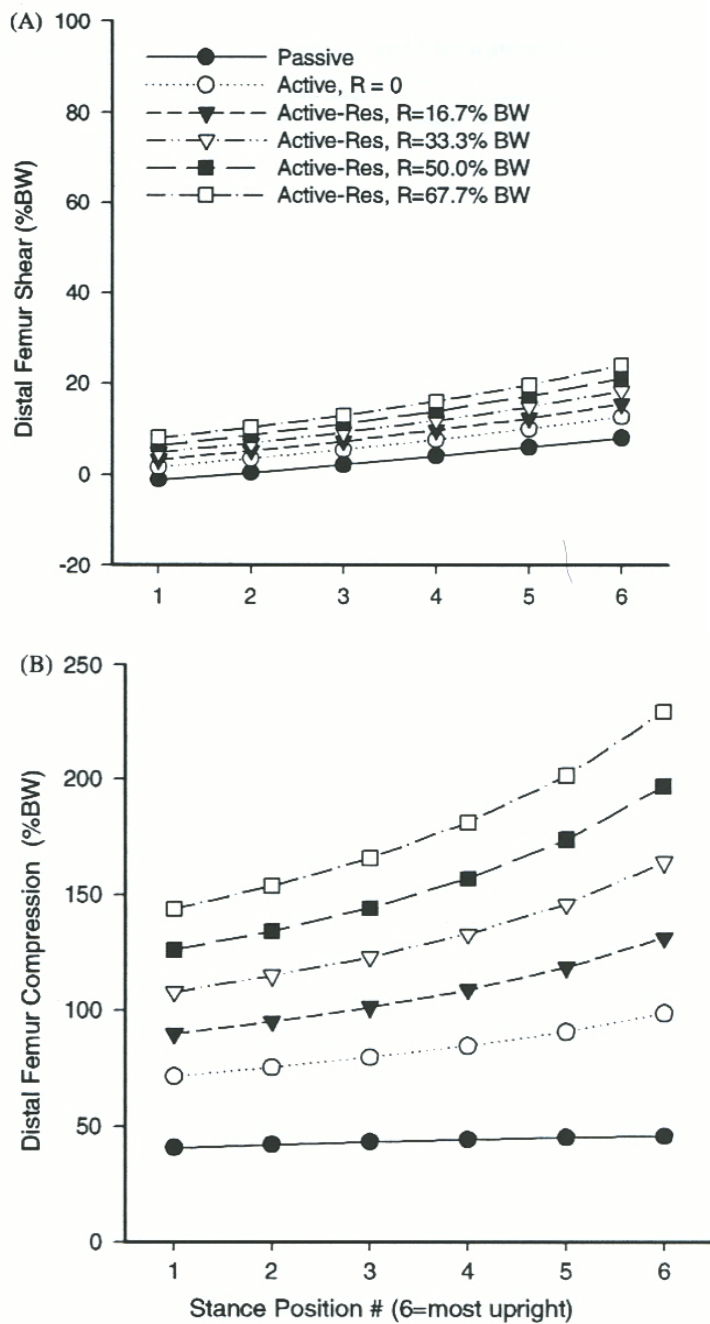
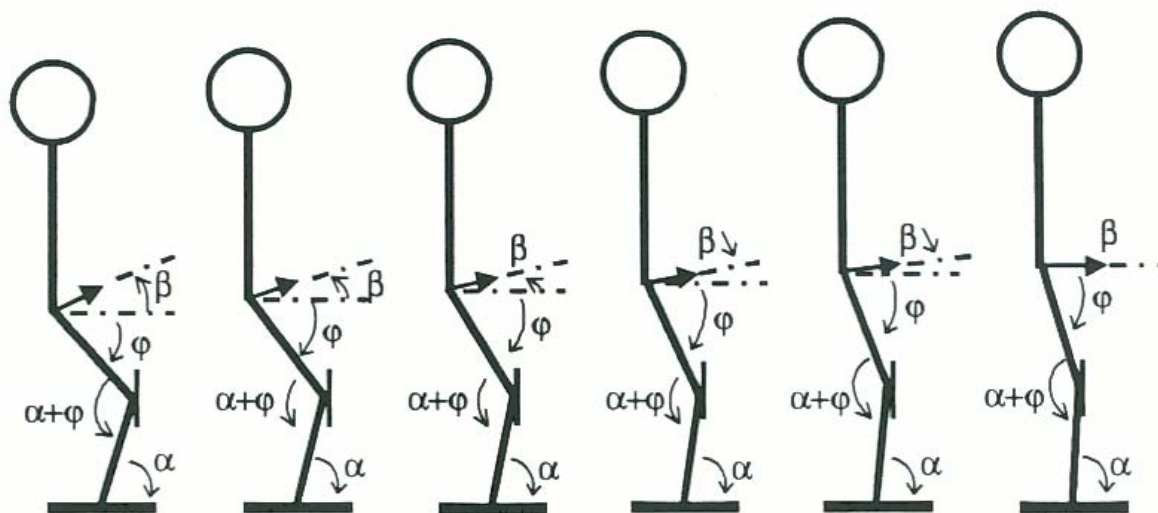


Figure 3. Modeled distal femur compression (A) and shear (B) in terms of percent body weight are plotted for passive, active, and active-resistive stance at each of the six stance postures. Note the different scales between graph A and B.

Source: Frey Law, L.A. and R.K. Shields, *Femoral loads during passive, active, and active-resistive stance after spinal cord injury: a mathematical model*. Clin Biomech (Bristol, Avon), 2004. **19**(3): p. 313-21.



Position #	1	2	3	4	5	6
Thigh angle (φ)	55°	59°	63°	67°	71°	75°
Shank angle (α)	75°	77°	79°	81°	83°	85°
Belt angle (β)	20°	16°	12°	8°	4°	0°

Figure 4. Schematic representations of six possible stance postures for individuals with spinal cord injury (SCI) using an external frame (not shown). The arrow at the hip and the vertical line at the knee represent a hip support belt and a knee support pad, respectively. The feet are placed on the ground.

Source: Frey Law, L.A. and R.K. Shields, Femoral loads during passive, active, and active-resistive stance after spinal cord injury: a mathematical model. Clin Biomech (Bristol, Avon), 2004. **19**(3): p. 313-21.

CHAPTER 3 METHODS

Mathematical Model

Supine Model

A two-dimensional, static, supine model has been developed to estimate the internal forces at the distal femur during FES, and to compare these compressive and shear forces to those in the standing model. The model assumes the human body is symmetric, and therefore, only one lower extremity was modeled. This model consists of the thigh, shank, and ankle represented as a three-bar linkage system (Fig. 5) which is consistent with the standing model. The model is assumed to act as a rigid body since only small deflections will occur when it is loaded by the quadriceps muscle group. The knee and ankle joints are modeled as two-dimensional, frictionless, pin joints and the hip joint is a fixed support in the x-direction, F_{xhip} , and the y-direction, F_{yhip} . Although the rectus femoris, one of the quadriceps muscles, crosses the hip, the internal moment at the hip was assumed to be negligible. The symbols, ϕ and α , are the angles from the vertical to the thigh and shank segment, respectively. The standing model used a variety of thigh and shank angles to examine six different positions of standing and Table 1 contains the values for ϕ and α . For both models, anthropometric values are used to determine the masses, W_{HAT} , W_{th} , W_{sh} , and W_{ft} , lengths, L_{th} , L_{sh} , and L_{ft} , and center of masses, CM_{th} and CM_{sh} of all of the segments from a hypothetical subject with height = 1.73 m and weight = 68.04 kg (See Appendix A) [47]. Although the mass of the thigh segment is fully supported, the distributed load was modeled as a single vector acting on the thigh. A force transducer is contained in the tibial restraint, R_A , at a length, L_m , from the knee joint which was arbitrarily chosen to be 0.400 meters. This force is perpendicular to the shank segment and, therefore its angle, β , changes as the shank angle changes and can be defined as $90^\circ - \alpha$.

When the quadriceps muscle is activated, it results in forces acting through the quadriceps tendon, F_{quad} , and patellar tendon, F_{pat} . While there is an internal moment at the

knee, it is due to the forces generated by the quadriceps, and therefore, is accounted for in the governing force and moment equations. The quadriceps muscles are modeled as a single vector as opposed to four vectors (one for each of the four quadriceps muscles). The supine model assumes that the horizontal components of F_{quad} and F_{pat} are equal and opposite [48, 49] because the vertical components of these forces in standing model were assumed to be equivalent. Also, since the internal angle of the quadriceps tendon and the patellar tendon is less than 10° [50], it can be assumed that the tendon forces act at a 5° angle from the thigh and shank segments, respectively (Fig. 6). The relationship between then quadriceps tendon and the patellar tendon is shown in Eq. 1.

$$F_{quad} \sin(\varphi - 5) = F_{pat} \sin(\alpha - 5) \quad (1)$$

For the seated and supine models, when the quadriceps muscles are stimulated the shank segment tries to extend but since it is fixed no movement actually occurs, resulting in an isometric contraction. Generally, it would be difficult to create a valid model of this isometric leg extension using FES or volitional control for a non-SCI individual. However, since those individuals with a complete SCI above the thoracic level do not have volitional control of their lower extremities then any internal muscle forces generated are due to FES, spasms, or passive tension. Therefore, by using FES, only the quadriceps muscles will be activated and while spasms could occur, unlike a non-SCI individual co-contractions of other muscle should not.

Supine Static Equilibrium Equations

The supine model is governed by three static equilibrium equations. These equations are sufficient to solve for the three unknown values, F_{xhip} , F_{yhip} , and R_A . The sum of all of the external forces in the x-direction equals zero (Eq. 2).

$$\sum F_x = 0; F_{xhip} - F_{quad} \sin(\varphi - 5) + F_{pat} \sin(\alpha - 5) + R_A \sin \beta = 0 \quad (2)$$

The sum of all of the external forces in the y-direction equals zero (Eq. 3).

$$\sum F_y = 0; F_{yhip} - W_{th} - F_{quad} \cos(\varphi - 5) - F_{pat} \cos(\alpha - 5) - W_{sh} + R_A \cos \beta - W_{ft} = 0 \quad (3)$$

The sum of all external moments equals zero (Eq. 4).

$$\begin{aligned} \sum M = 0; & -W_{th}(L_{th} - CM_{th}) \sin \varphi - (F_{quad} \cos(\varphi - 5) + F_{pat} \cos(\alpha - 5))(L_{th} \sin \varphi) \\ & + (F_{quad} \sin(\varphi - 5) - F_{pat} \sin(\alpha - 5))(L_{th} \cos \varphi) - W_{sh}(L_{th} \sin \varphi + CM_{sh} \sin \alpha) \\ & + R_A \cos \beta(L_{th} \sin \varphi + L_m \sin \alpha) - R_A \sin \beta(L_{th} \cos \varphi + L_m \cos \alpha) \\ & - W_{ft}(L_{th} \sin \varphi + L_{sh} \sin \alpha + L_{ft}) = 0 \end{aligned} \quad (4)$$

These equations for were solved for F_{xhip} , F_{yhip} , and R_A using Matlab computer software (Prentiss Hall, New Jersey, USA) and the computer code is located in Appendix B. The external forces, segment mass and muscles forces were known along with moment arms, segment length and center of mass of the segments. Since the location of the force transducers changes between the standing model and the supine model, it was necessary to have the degree of muscle activation remain uniform. In order to accurately compare these models, the quadriceps force and thereby the patellar force (Eq. 1) from the standing model were used in the supine model.

Supine Compression and Shear Equations

The solutions from the previous equilibrium equations can be used to determine the internal shear and compressive forces at the distal femur for the supine model. The thigh segment was cut or sectioned at the distal femur, 85% of the length of the thigh segment measured from the hip. These internal forces in the femur were examined at a femur length of 85% from the hip because it is the common site of fracture in individuals with SCI [9] (Fig. 7). Compressive force (F_c) and shear force (F_v) were estimated using the following equations (Eq. 5) and (Eq. 6) and the femur was assumed to be of uniform material at this location.

$$-F_{xhip} \sin \varphi - F_{yhip} \cos \varphi - F_{quad} \cos(5) + 0.85W_{th} \cos \varphi + F_c = 0 \quad (5)$$

$$F_{xhip} \cos \varphi - F_{yhip} \sin \varphi + F_{quad} \sin(5) - 0.85W_{th} \sin \varphi + F_v = 0 \quad (6)$$

Seated Model

In order to evaluate the second hypothesis, a two-dimensional, static, seated model was developed. Similar to the supine model, a three-bar linkage system was used for the lower extremity, the knee and ankle joints were modeled as frictionless, pin joints, and the hip joint was a fixed support. The seated model (Fig. 8) also measures force at the distal tibia (R_A) like the supine model but it and the distance from the knee joint (lateral femoral condyle) to the transducer (L_m) are determined experimentally. The force at the tibial restraint is assumed to be normal or perpendicular to the shank segment. Also, the knee angle or the angle between the thigh and shank segments is 90° . The quadriceps muscle, F_{quad} , is directed towards the hip and is 5° from the thigh segment, like the supine model.

Seated Static Equilibrium Equations

The external forces F_{xhip} , F_{yhip} and, F_{quad} need to be determined before the internal forces at the distal femur can be estimated. The mass of the segments, W_{HAT} , W_{th} , W_{sh} , and W_{ft} , are based on body weight and determined using anthropometric values. The thigh segment length, L_{th} , and the center of mass of the thigh segment, CM_{th} , also implement anthropometric values but are based on height. R_A and L_m are determined experimentally. The sum of all of the external forces in the x-direction equals zero (Eq. 7).

$$\sum F_x = 0; F_{xhip} - F_{quad} \cos(5) + R_a = 0 \quad (7)$$

The sum of all of the external forces in the y-direction equals zero (Eq. 8).

$$\sum F_y = 0; F_{yhip} - 0.5W_{hat} - F_{quad} \sin(5) - W_{th} - W_{sh} - W_{ft} = 0 \quad (8)$$

The sum of all of the external moments equals zero (Eq. 9).

$$\sum M = 0; -W_{th}(L_{th} - CM_{th}) - F_{quad} \sin(5)(L_{th}) + R_a L_m - (W_{sh} + W_{ft})(L_{th}) = 0 \quad (9)$$

The equilibrium equations of the seated model were solved using Matlab and the programming code is contained in Appendix C.

Seated Compression and Shear Equations

Once the condition equations of the seated model were solved, these solutions were used to estimate the compressive and shear forces at the distal femur. Again, these internal forces were evaluated at a common fracture site for SCI individuals, 85% of thigh length from the hip joint. Because of the angle of knee flexion, the axes of the compressive and shear forces correspond with the Cartesian coordinate system (Fig. 9). These internal forces were estimated using Eq. 10 to determine the compressive force and Eq. 11 to solve for the shear force.

$$-F_{xhip} - F_{quad} \cos(5) + F_c = 0 \quad (10)$$

$$0.5W_{hat} - F_{yhip} + 0.85W_{th} - F_{quad} \sin(5) + F_v = 0 \quad (11)$$

Experimental Testing Conditions

Supine Model

In order to validate the supine model, FES was delivered to the quadriceps muscle of a non-SCI subject during both the standing and supine models. The quadriceps muscles were activated using 7 x 13 cm, carbon, surface electrodes placed at the proximal and distal end of the thigh segment. The experimenter placed the distal electrode proximal to the most distal palpable border of the vastus lateralis and the proximal electrode was placed as close as possible to the inguinal crease. The electrodes were positioned medial to the abductor muscle group and lateral to the adductor group (Fig. 10).

A male subject without SCI, with a height of 1.75 m and a mass of 90.9 kg, was used to examine the supine model. The subject signed an informed consent document approved by the University of Iowa human subjects institutional review board. The subject first completed the standing exercise at the third position with the thigh angle of 63° and a shank angle of 79°. Only one position was chosen to validate the model in order to ensure that the quadriceps muscle group did not fatigue during the protocol and thereby confound the results. The position of the subject was verified manually using a goniometer to measure the

angle of the knee. A current of 90 mA was chosen because it produced a sufficient force reading and was well tolerated by the subject without spinal cord injury. Also, the supine model predicted high shear forces during high quadriceps muscle force; therefore, a low current of 90 mA was used to activate the muscle in case these predictions were accurate. Five trains were delivered to the quadriceps muscle using an Infinity Plus Clinical Portable Electrotherapy system (Empi, St. Paul, MN). The trains had a frequency of 20 Hz for a duration of 5 seconds followed by 5 seconds of rest. The stimulus pulse width was 200 microseconds. The force generated by the quadriceps muscle was measured by a force transducer at the knee (Interface 1500 ASK-200, Scottsdale, AZ). Using the peak force of the five trains and the mathematical standing model, the quadriceps muscle force was obtained.

The subject was then asked to lay supine with the same lower extremity position as the standing model to examine the supine model (Fig. 11). The electrodes remained in the same position as the standing protocol and therefore the same amount of current should yield the same quadriceps muscle force. A belt was safely fastened across the subject's abdomen to secure his trunk. The leg was attached to the mechanical arm of the isokinetic dynamometer (KinCom) using a padded strap that passed behind the posterior surface of the shank and pulled it into contact with the transducer. The transducer was contained in the mechanical arm of the KinCom and cups the anterior surface of the shank. The adjustability of the mechanical arm and the height of the seat allowed at the hip and the knee positions to be easily changed. The third position, with respect to thigh angle and shank angle, from the standing model was simulated in the supine position. Once the subject was secured to the KinCom, a goniometer was used to manually verify the segment angles and any adjustments to position were made.

The quadriceps muscle was activated using the same stimulator as the standing model with the same 90 mA current. The stimulator delivered five 20 Hz trains for 5 seconds followed by 5 seconds of rest. The force at the tibial restraint, R_A , was recorded and compared to the force obtained from the mathematical supine model.

Seated Model

Experimental measurements need to be collected as parameter inputs for the mathematical seated model. One SCI male was asked to participate in the doublet stimulation protocol [43]. The subject remained in his wheelchair throughout the collection (Fig.12). The subject signed an informed consent document approved by the University of Iowa human subjects institutional review board. The anterior surface of the ankle was in contact with the force transducer (1500ASK-200, Interface, Scottsdale, AZ). The distance from the force transducer to the lateral femoral condyle was measured and recorded as the moment arm. The subject was positioned so that the knee was in 90° of flexion which was verified manually using a goniometer. Surface electrodes were positioned over the quadriceps muscle using the same placement method as the supine model. The previous publication [43] concluded that the peak force elicited by a doublet occurred at a frequency of 30 Hz. While the entire doublet force-frequency curve was completed to gain insights into the muscle physiology of the subject's quadriceps muscle, only the 30 Hz condition was used for this project. At 30 Hz, three doublets were delivered to the quadriceps muscle, separated by 2 seconds of rest.

Data Collection and Analysis

For all three experimental protocols, the analog force signal was amplified and converted to a digital signal using 12-bit resolution analog-to-digital converter with a sampling rate of 2,000 samples per second. Datapac 2K2 software (RUN Technologies, Mission Viejo, CA) was used to analyze the digital force signals. The five peak forces (the maximum amplitude of the force signal) for the standing and the supine models were determined and averaged. The peak forces from the three doublet twitches were also averaged and recorded.

Position	1	2	3	4	5	6
φ	55°	59°	63°	67°	71°	75°
α	75°	77°	79°	81°	83°	85°

Table 1. The six supine positions with the corresponding thigh angle (φ) and shank angle (α).

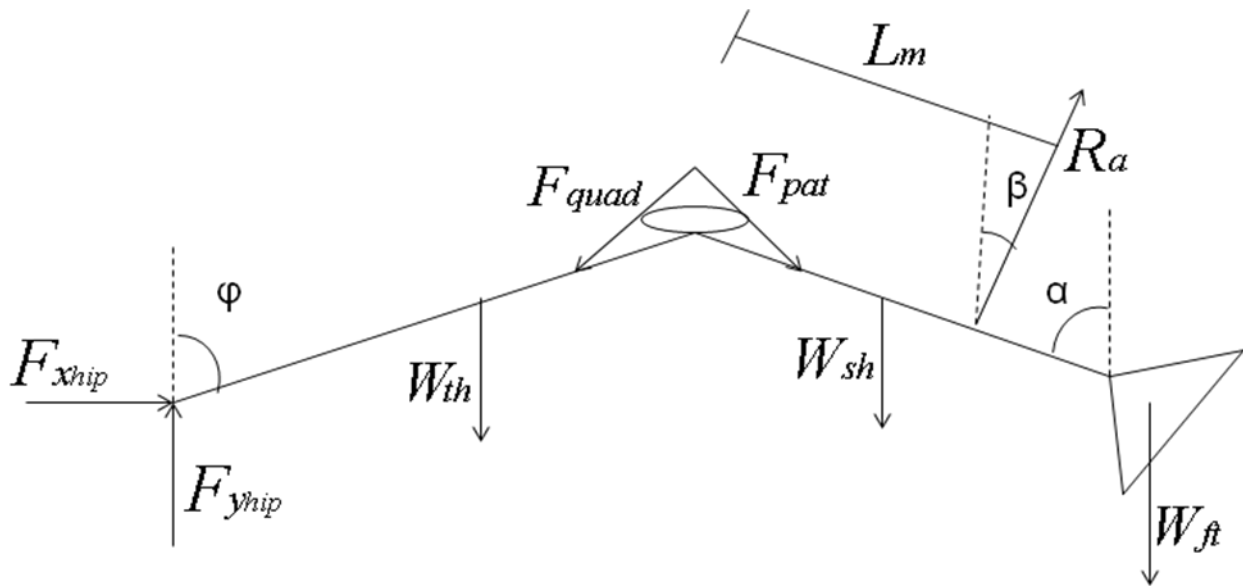


Figure 5. Schematic free body diagram of the external forces and loading conditions acting on the lower extremity for the supine model.

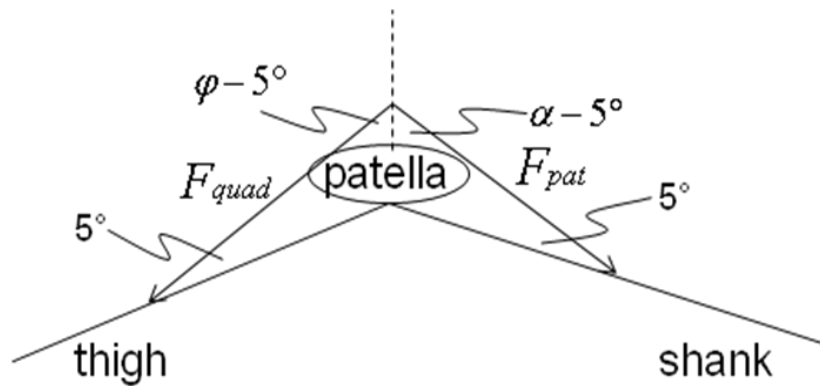


Figure 6. Schematic representation of the relationship between the quadriceps tendon or muscle (F_{quad}) and the patellar tendon (F_{pat}) at the knee joint.

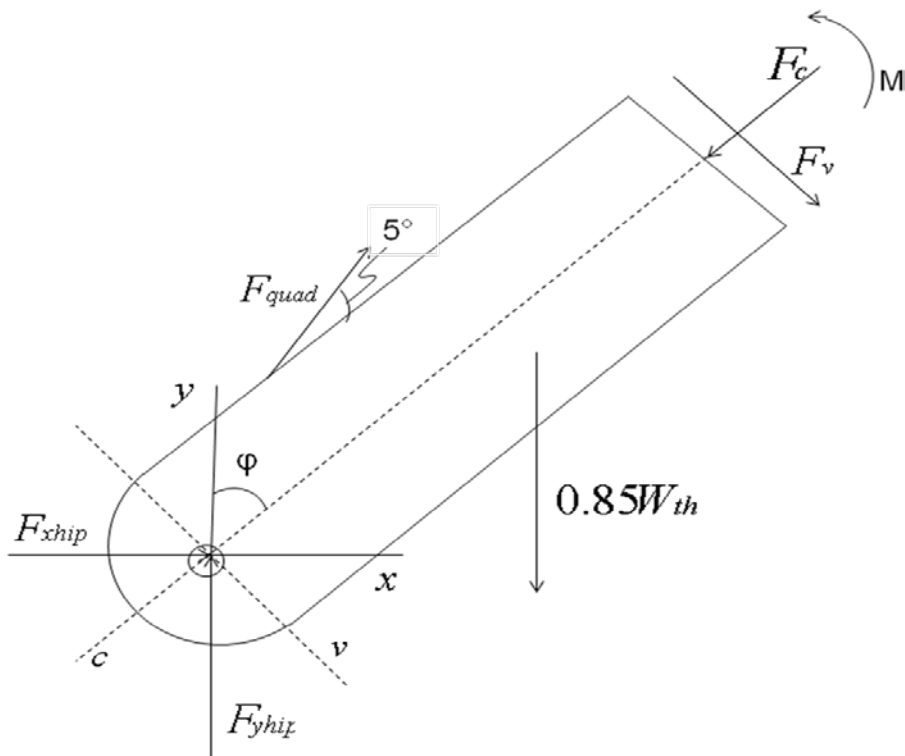


Figure 7. Schematic free body diagram of the distal femur for the supine model which has been cut at 85% of thigh segment length from the hip joint. The bending moment at the distal femur was not determined but the compressive force (F_c) and shear force (F_v) were calculated.

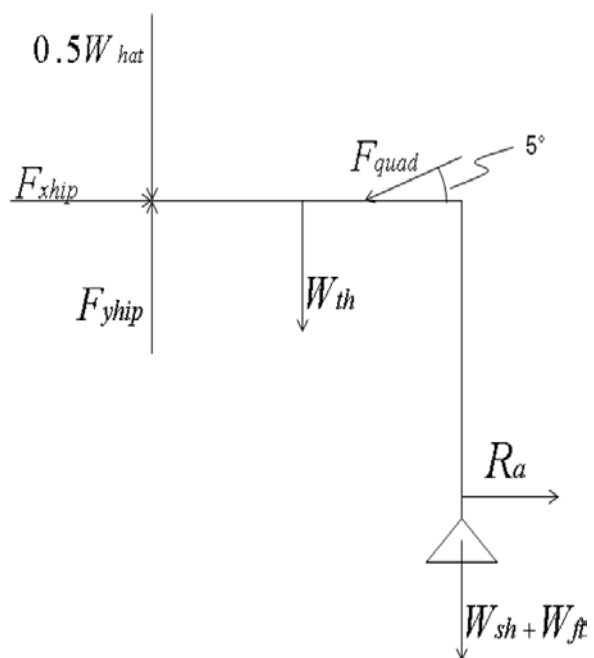


Figure 8. Schematic free body diagram of the external forces and loading conditions acting on the lower extremity for the seated model

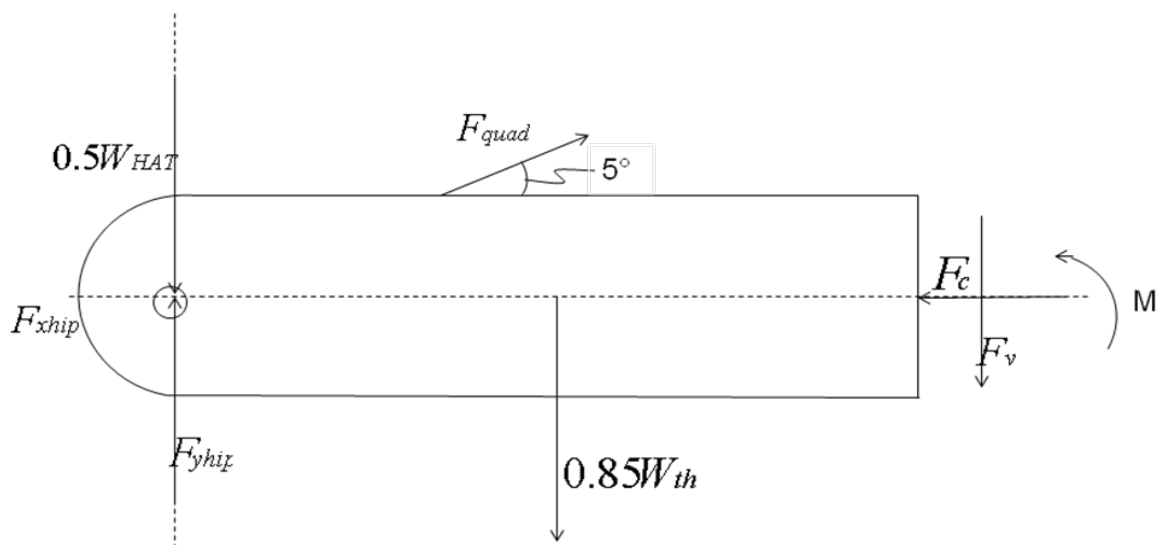


Figure 9. Schematic free body diagram of the distal femur for the seated model which has been cut at 85% of thigh segment length from the hip joint. The bending moment at the distal femur was not determined but the compressive force (F_c) and shear force (F_v) were calculated.

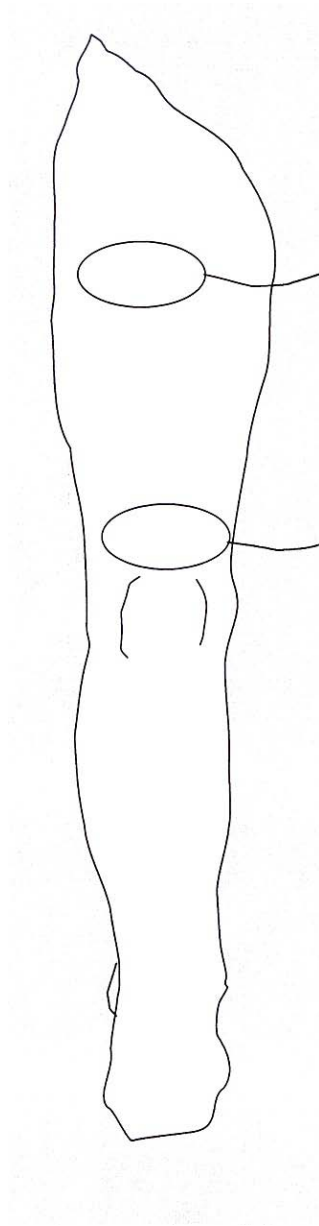


Figure 10. Placement of surface electrodes over the quadriceps muscle.

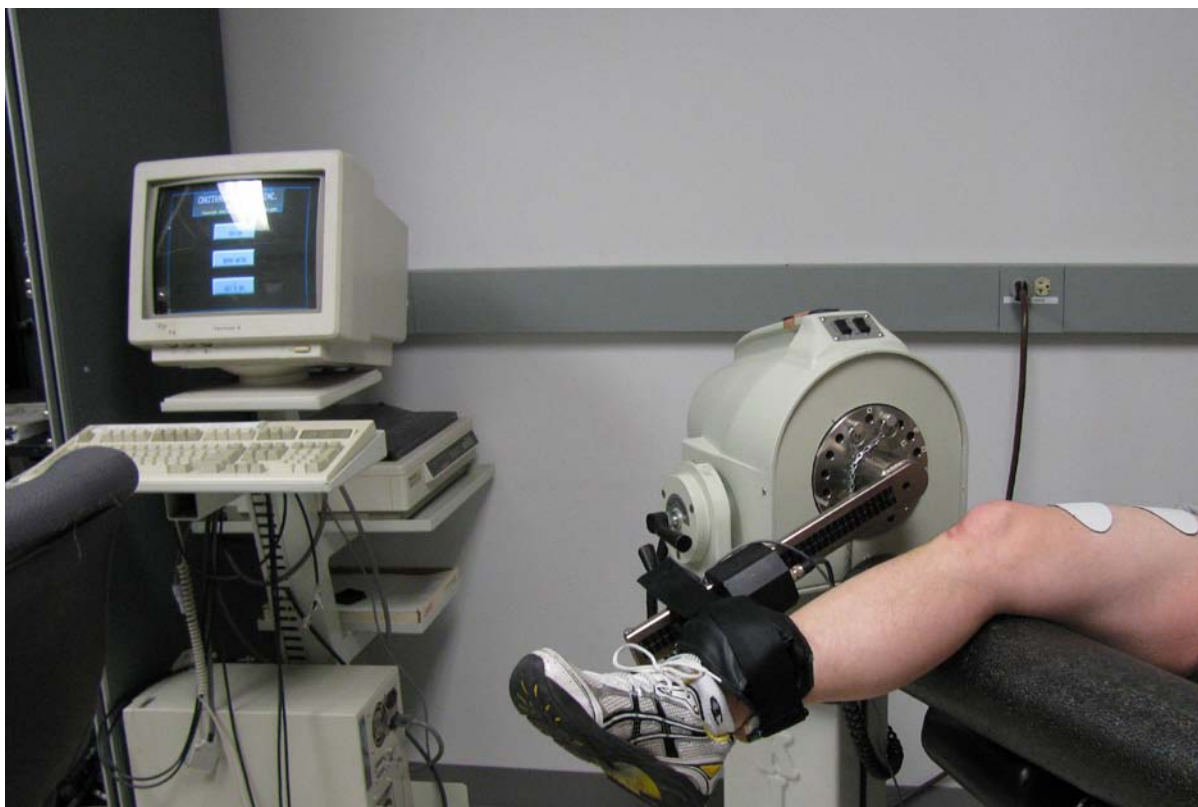


Figure 11. Non-SCI male positioned on the KinCom for the experimental supine model.

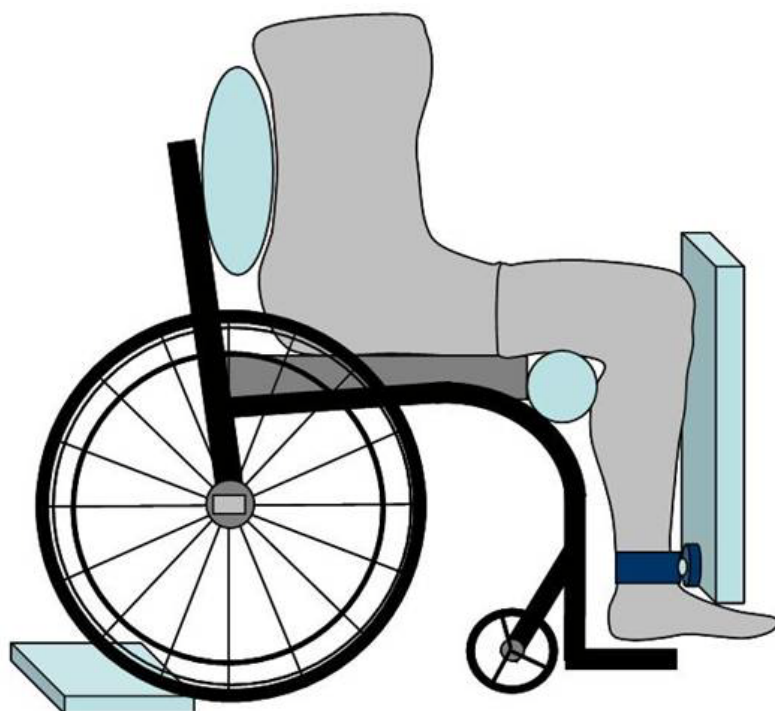


Figure 12. Schematic of the experimental seated model of the doublet stimulation protocol.

CHAPTER 4 RESULTS

Experimental Results

The mathematical model for the seated position required the tibial restraint force and the moment arm to be determined experimentally. A SCI individual was positioned in his wheelchair with his knee in 90° of flexion. The distance from the lateral femoral condyles to the force transducer at the distal tibia was measured and recorded as 0.321 m. The peak force for the doublet quadriceps muscle contraction occurred at 30 Hz and was equivalent to 13.3 kg. The subject's height and weight are 1.93 m and 70.45 kg, respectively. The peak force and moment arm for the tetanic quadriceps muscle contraction are 20.8 kg and 0.451 m, respectively, and these were taken from the Hartkopp study which resulted bone fracture [41]. Since the height and weight of the subject were not cited in the manuscript, the hypothetical subject weight of 68.04 kg and height of 1.73 m were used.

Mathematical Model Predictions

Supine Model Predictions

The model condition equations were used to solve for the three unknowns of the system, R_A , F_{xhip} , F_{yhip} . The force at the tibial restraint and the horizontal and vertical forces at the hip are plotted in Figs. 13, 14, and 15, respectively, at six supine positions with five different quadriceps muscle forces at each position. The tibial restraint force increases as quadriceps muscle force increases and ranges from 21.2% to 61.7% of body weight. Position 1 has the highest tibial restraint forces for each of the five groups of quadriceps force compared to the other positions with position 6 having the lowest forces. However, the horizontal force at the hip is inversely related to the quadriceps force and has a range of -1.84% to -16.0% of body weight. For the horizontal force, position 1 has the largest magnitude of force compared to the other positions in each of the five groups of forces with position 6 having the lowest magnitude. The vertical force at the hip ranges from 21.2% to

54.1% and is directly related to the quadriceps force. Position 6 and position 1 have the highest and lowest vertical forces, respectively, compared to the other positions in each of the five clusters.

The values determined by the equilibrium equations were used to calculate the compressive and shear forces at the distal femur which are plotted in Figs. 16 and 17, respectively. The compressive force is positively correlated to quadriceps force. It ranges from 33.1% of body weight at position 1 to 191.1% of body weight at position 6. Shear force increases as the quadriceps force increases and ranges from 16.7% to 61.5% of body weight. At position 6, the distal femur experiences the highest amount of shear force compared to the other positions and position 1 has the lowest shear force. In position 6, the leg is almost fully extended and therefore has the longest moment arm.

Figure 18 shows all of five variables; tibial restraint force, the horizontal and vertical forces at the hip, and the compressive and shear forces at the distal femur at position 1. The tibial restraint force, vertical force at the hip, and shear force at the distal femur have a similar relationship and all show a slight increase as the amount of quadriceps force increases. The horizontal force at the hip is much lower than the other forces and has indirect relationship with the quadriceps force. The compressive force at the distal femur has the largest magnitude of all the variables and has the greatest amount of increase with respect to quadriceps force. Since all of the positions have similar trends and inter-variable relationships, position 1 is shown as a representative example.

Supine and Standing Model Comparisons

In order to examine the internal forces at the distal femur, the compressive and shear forces for both supine and standing mathematical models were plotted. It was predicted that the standing model would estimate higher compressive force and lower shear forces at the distal femur compared to the supine model. The compressive forces of the supine model and the standing models are plotted against quadriceps force in Fig. 19. The standing model

predicts much higher compressive force compared to the supine model. The compressive force of the standing model ranges from 75% to 240% of body weight. In order to discern which values in the supine model correspond to the standing model, the compressive force is also graphed by position in Fig. 20 but Fig. 21 is a representative example of compressive force at the first position which is much clearer than Fig 20. Fig. 21 shows the compressive forces of the supine and standing model at the distal femur. At each position, the standing model had higher compressive force than the supine model which was expected because the supine model excludes the weight of the trunk, head, and upper body.

Shear force was also examined in Figs. 22-24 similarly to compressive force. Figure 22 shows that the supine model estimated more shear force at the distal femur compared to the standing model. While it is easy to see that the supine model tended to have more shear force, it is difficult to match the quadriceps force corresponding to each model so Fig. 23 plotted the models by position. The graphs are separated further to only show one position, Fig. 24, which plots the shear force of both models at the first position. Since all of the positions follow a similar pattern only position 1 is included. At each particular quadriceps force, the supine model estimates more shear in the distal femur than the standing model. This is true because in the supine model the force opposing the quadriceps muscle is acting at the distal tibia, the tibial restraint, and in the standing model this force is at the knee. In the supine model, the point of resistance is more distal than the standing model and this increased distance from the force transducer to the hip corresponds to an increase in shear force.

Seated Model Predictions

A seated model was developed to determine how the forces at the distal femur differ between a tetanic contraction and a doublet pulse to the quadriceps muscle. It was hypothesized that at 90° of knee flexion, tetanic activation of the quadriceps muscle would result in higher compressive and shear forces at the distal femur. The three independent,

equilibrium equations from the seated model and then compressive and shear equations were solved to determine the five unknowns of the system. The quadriceps muscle force, the horizontal and vertical forces at the hip, and, the compressive and shear forces at the distal femur for both types of stimuli are shown in Table 2. All of the forces are much higher for the tetanic muscle contractions compared to the doublet contractions with a compressive force of 477% of body weight and a shear force of 68.6% body weight. However, the compressive and shear forces that resulted from a doublet pulse were 38.3% and 29.3% body weight, respectively. These results support the second hypothesis and are not surprising because the doublet pulse results in a much lower quadriceps force than the tetanic contraction.

Validity of Mathematical Models

In order to determine the accuracy a mathematical model, it needs to be validated through experimental testing. Because the supine and the seated model are estimating the compressive and shear forces at the distal femur, validation cannot be performed non-invasively. However, validation of the force at the tibial restraint for the supine model could be tested. The predicted force at the tibial restraint determined by the quadriceps force from the standing model was 26.6 kg or 29.3% of body weight. The force measured at the tibial restraint during the experimental supine position was 25.7 kg or 28.3% of body weight. The percent error calculated between the predicted value and the experimental value was 3.4%.

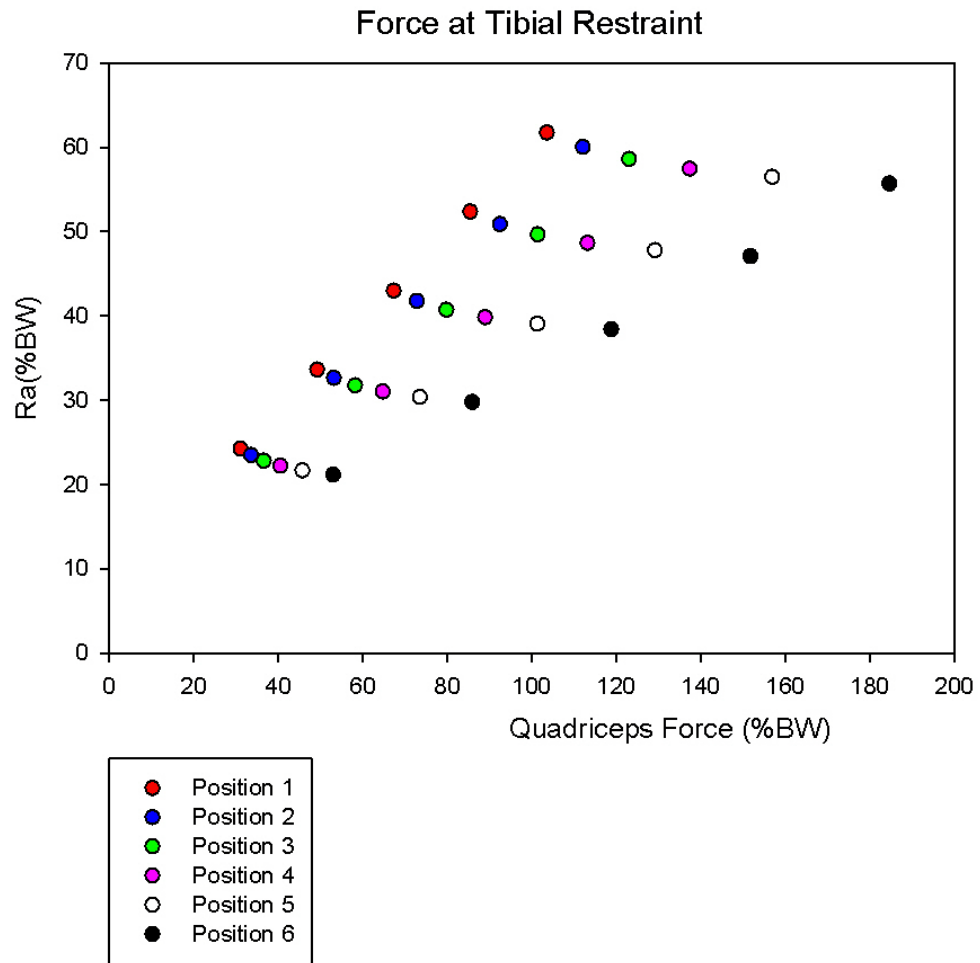


Figure 13. The supine model predictions for the forces at the tibial restraint, R_A , at various quadriceps muscle forces for the six different supine positions are graphed in terms of percent body weight (%BW).

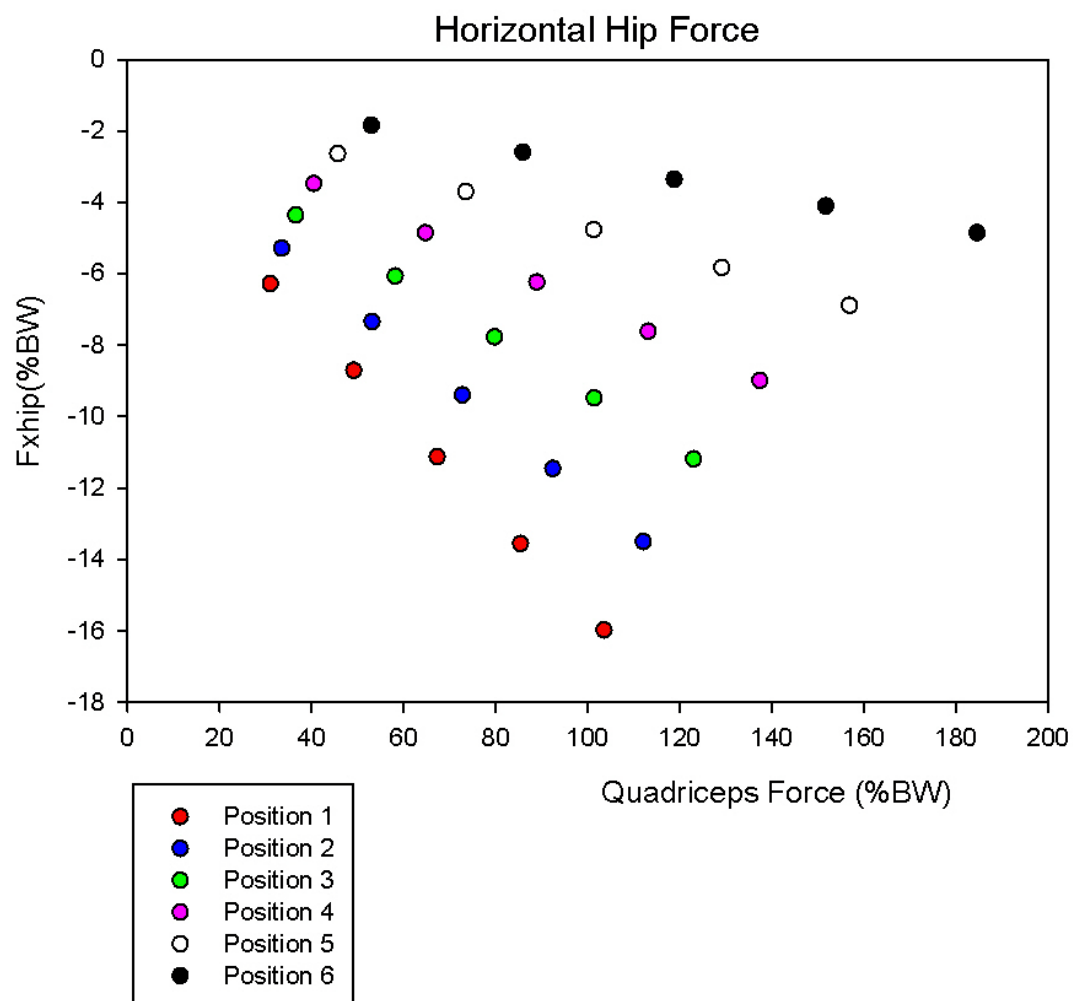


Figure 14. The estimates of the horizontal forces at the hip, F^{xhip} , for the supine model at various quadriceps muscle forces for the six different supine positions are plotted in terms of percent body weight (%BW).

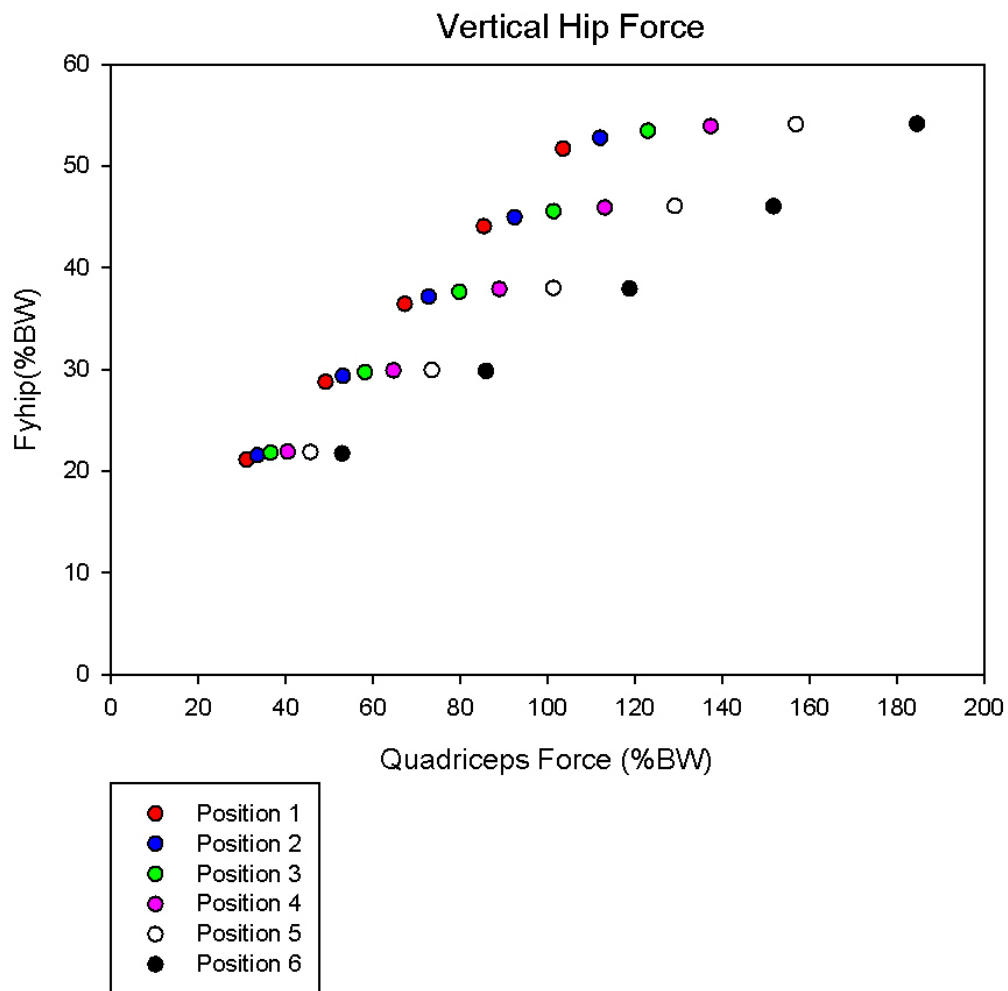


Figure 15. The supine model estimates of the vertical forces at the hip, F_{yhip} , are plotted in terms of percent body weight (%BW) for the six supine position with five different quadriceps muscle forces at each position.

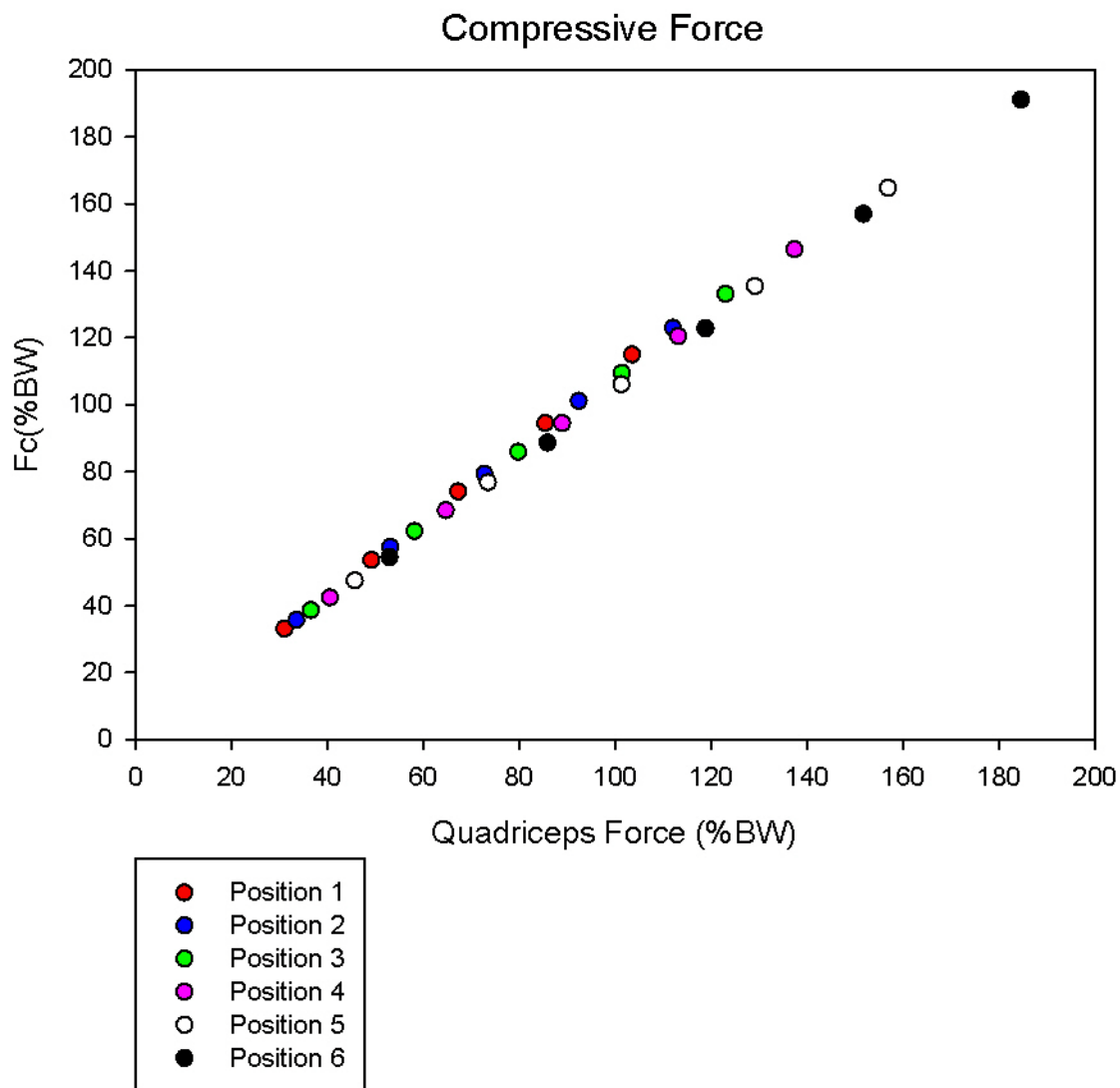


Figure 16. The compressive forces, F_c , estimated at the distal femur for the supine model in percent body weight (%BW) and graphed against quadriceps force.

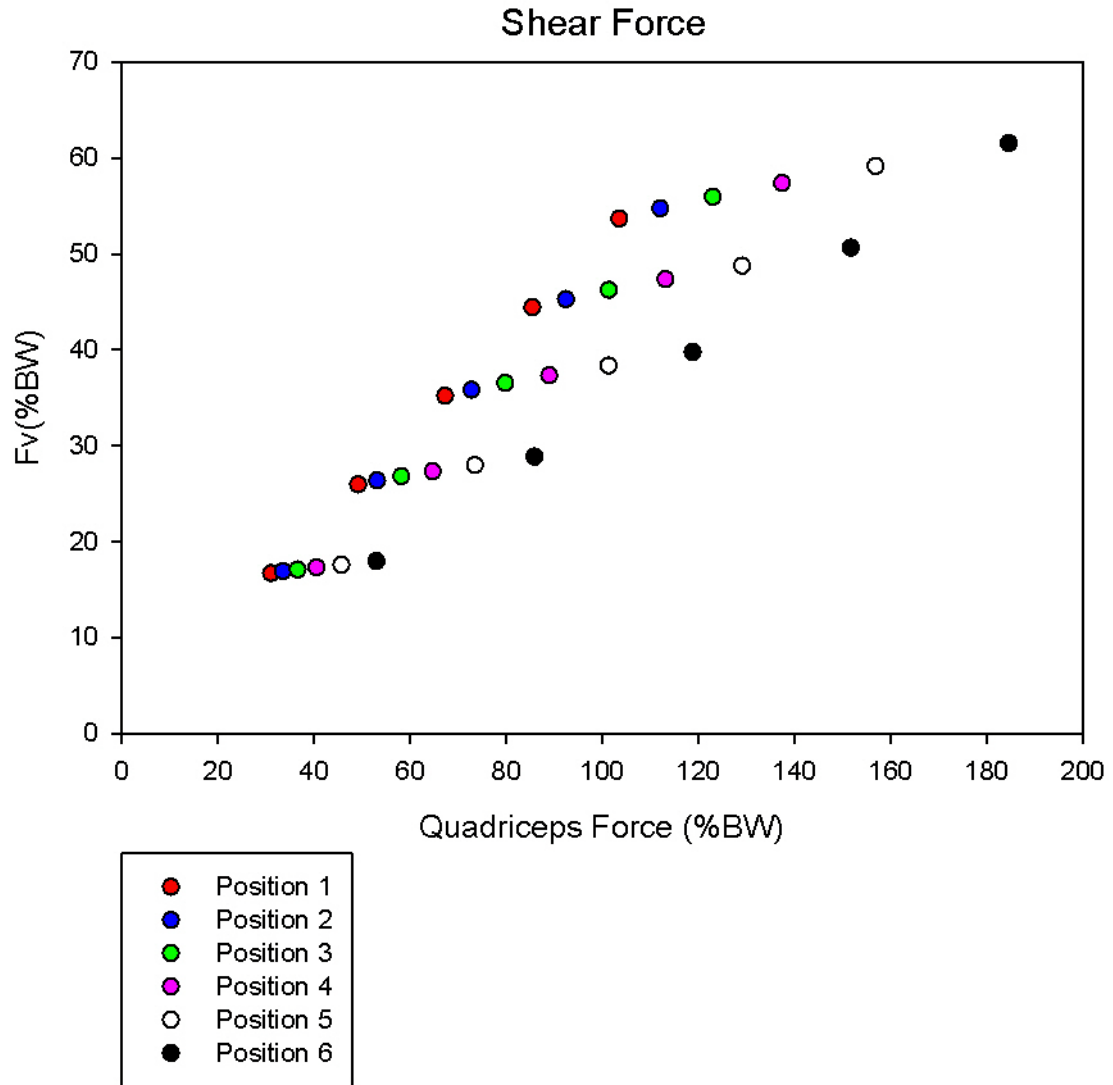


Figure 17. The shear forces, F_v , estimated at the distal femur for the supine model in percent body weight (%BW) and graphed against quadriceps force.

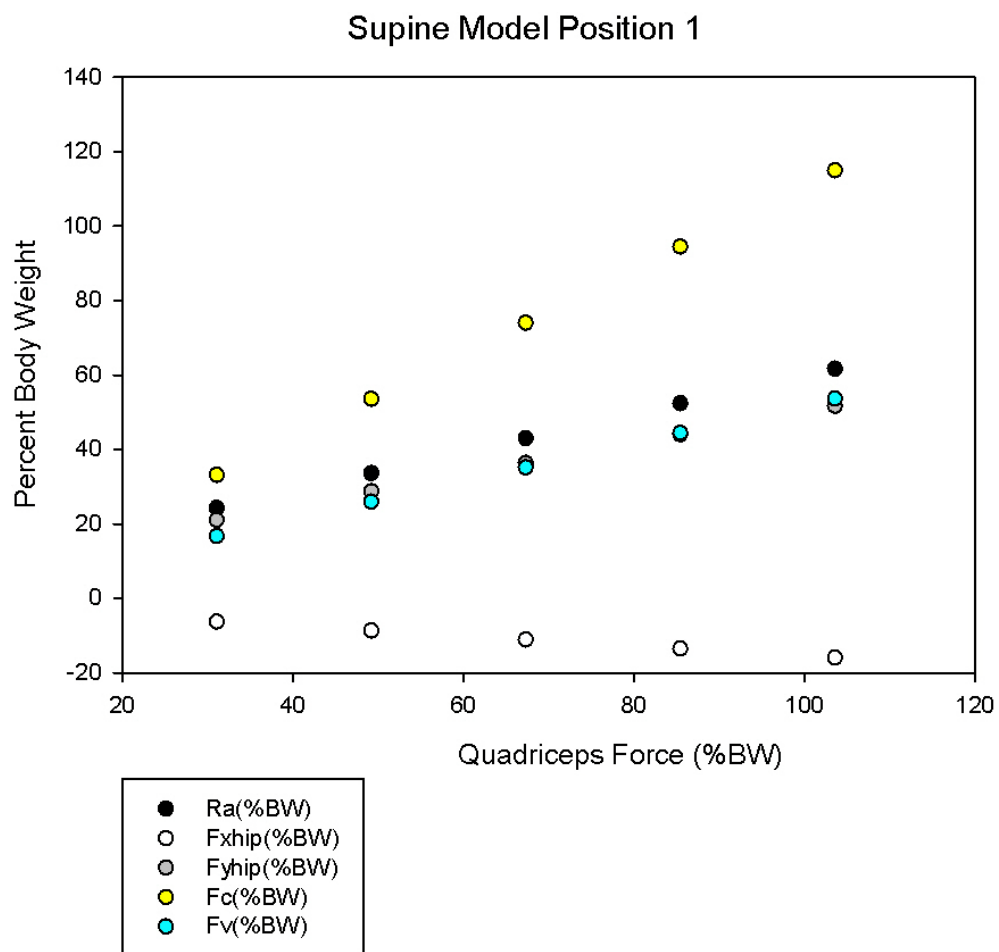


Figure 18. The estimates from the supine model for the tibial restraint force, the horizontal and vertical forces at the hip, and the compressive and shear forces at the distal femur for position 1 at five quadriceps forces.

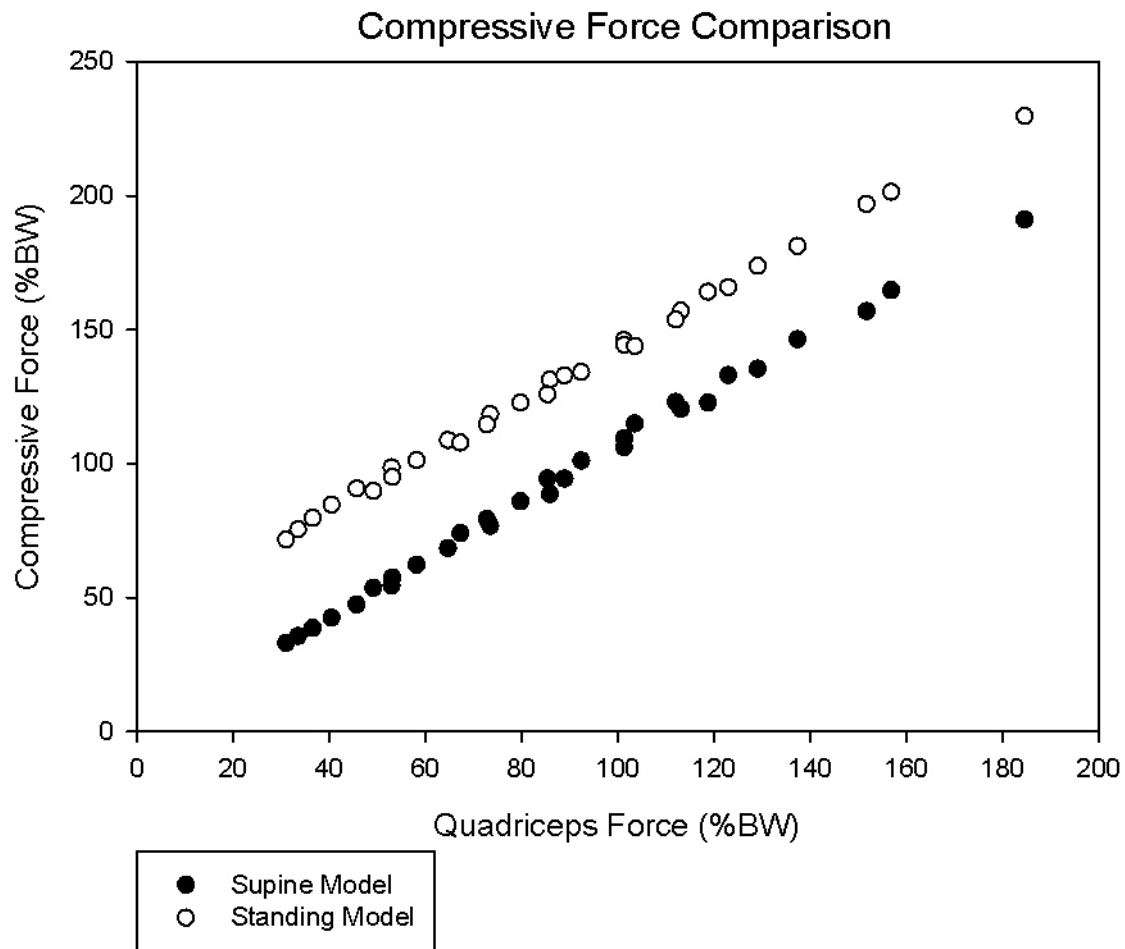


Figure 19. The compressive forces at the distal femur for the supine model and the standing model are plotted in terms of body weight (%BW) with respect to quadriceps muscle force.

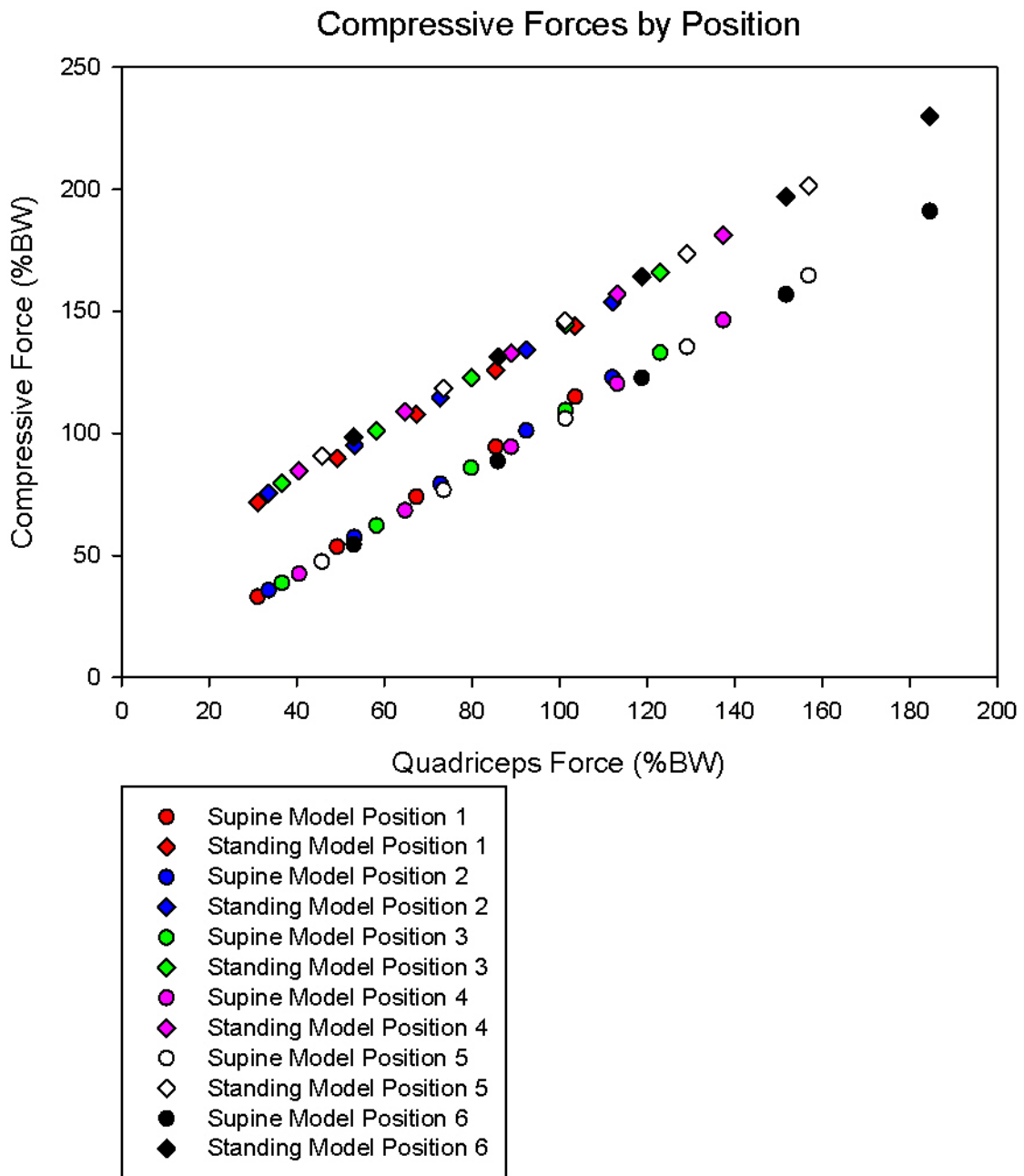


Figure 20. Compressive forces at the distal femur of the supine and standing models separated by position and plotted in terms of percent body weight (%BW)

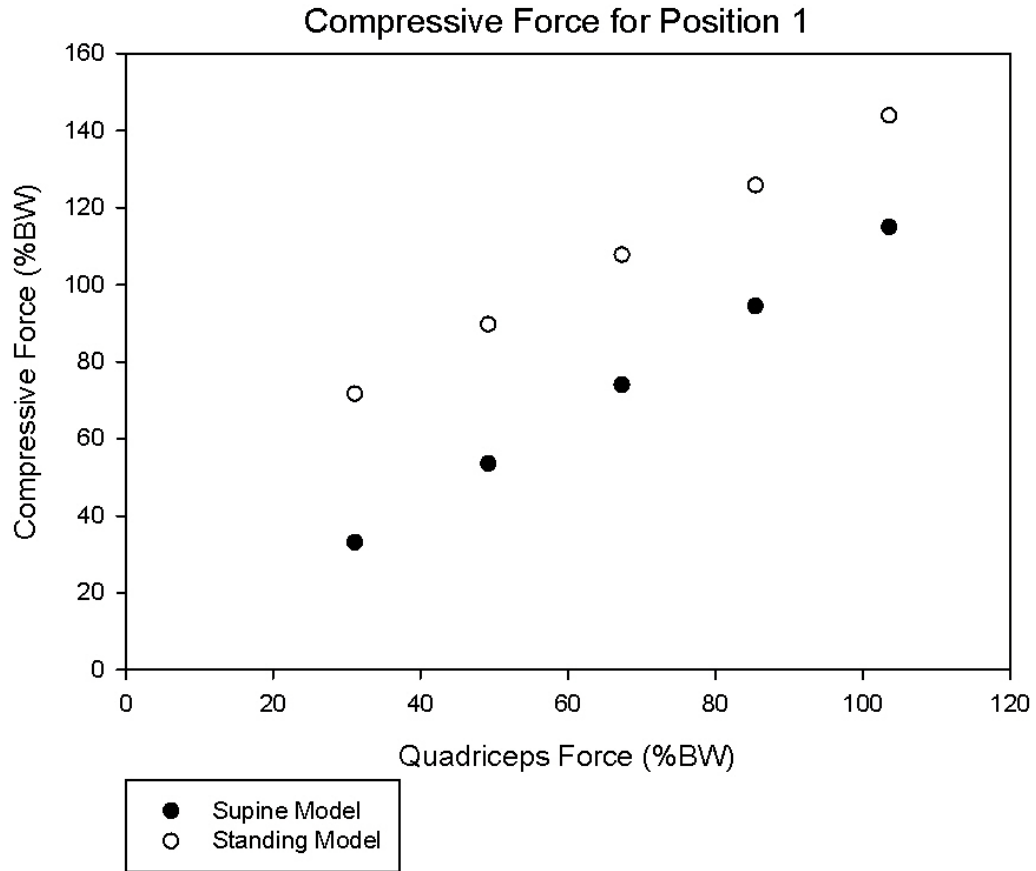


Figure 21. A representative example of the compressive forces at the distal femur of position 1 for the supine and standing models as a percent of body weight (%BW) plotted against quadriceps muscle force.

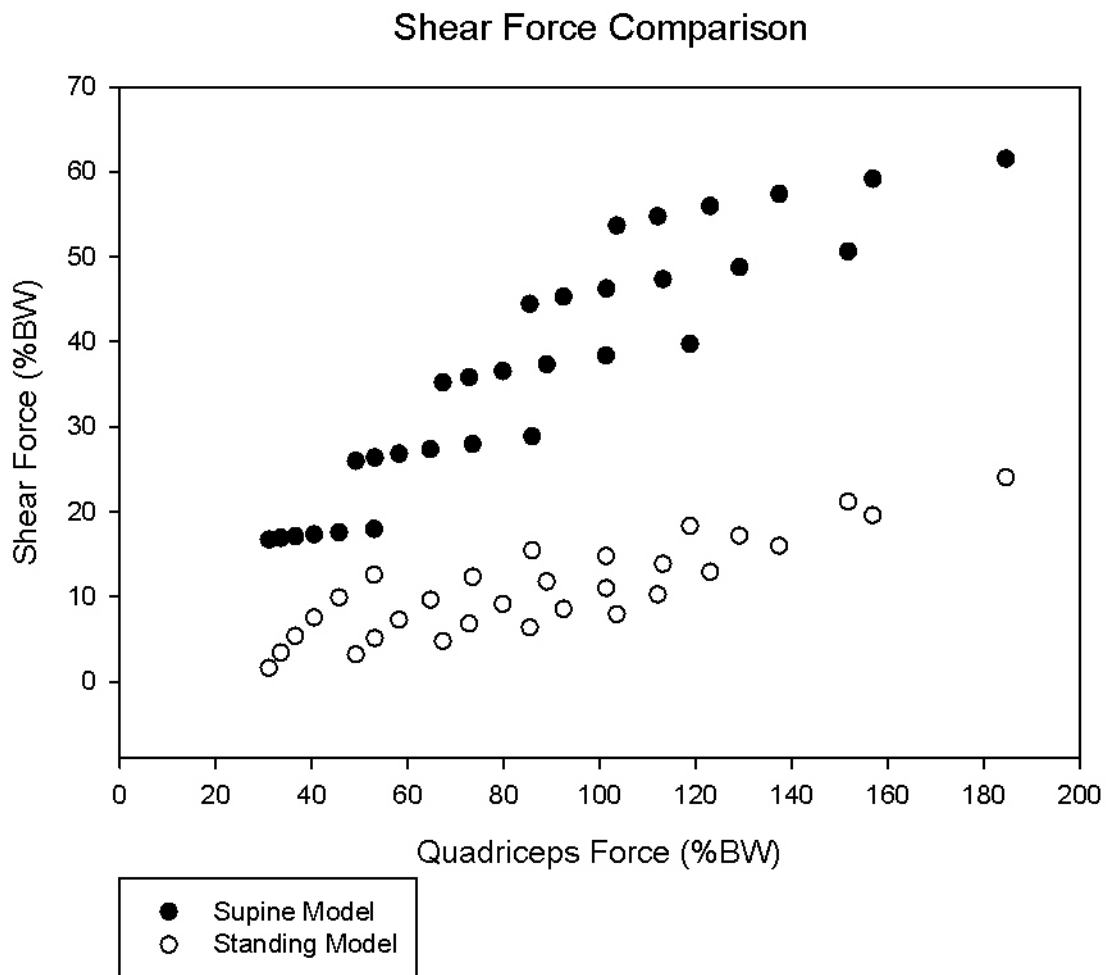


Figure 22. The shear forces at the distal femur for both models, supine and standing, are plotted in terms of percent body weight (%BW) as a function of quadriceps muscle force.

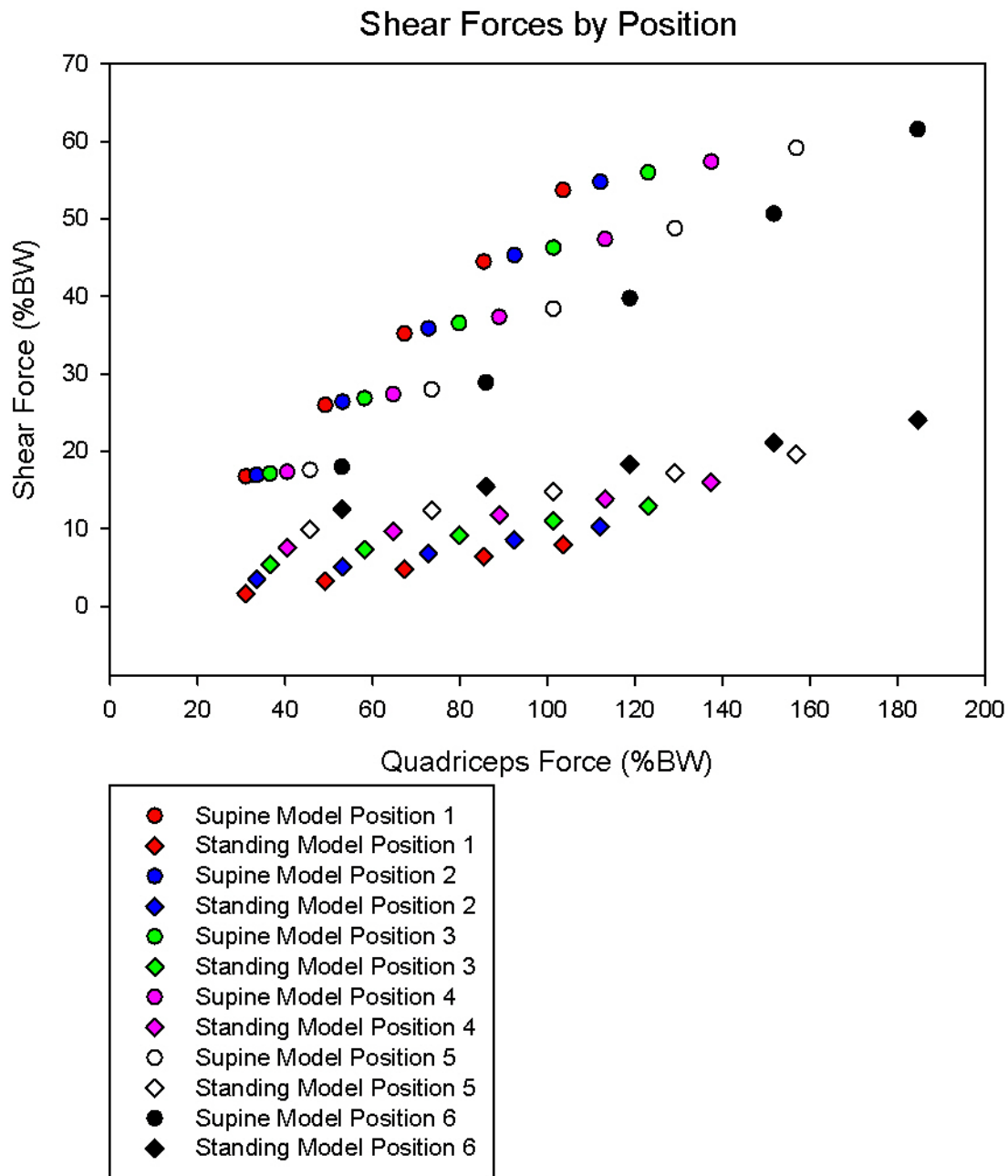


Figure 23. Shear forces at the distal femur of the supine and standing model separated by position and plotted in terms of percent body weight (%BW).

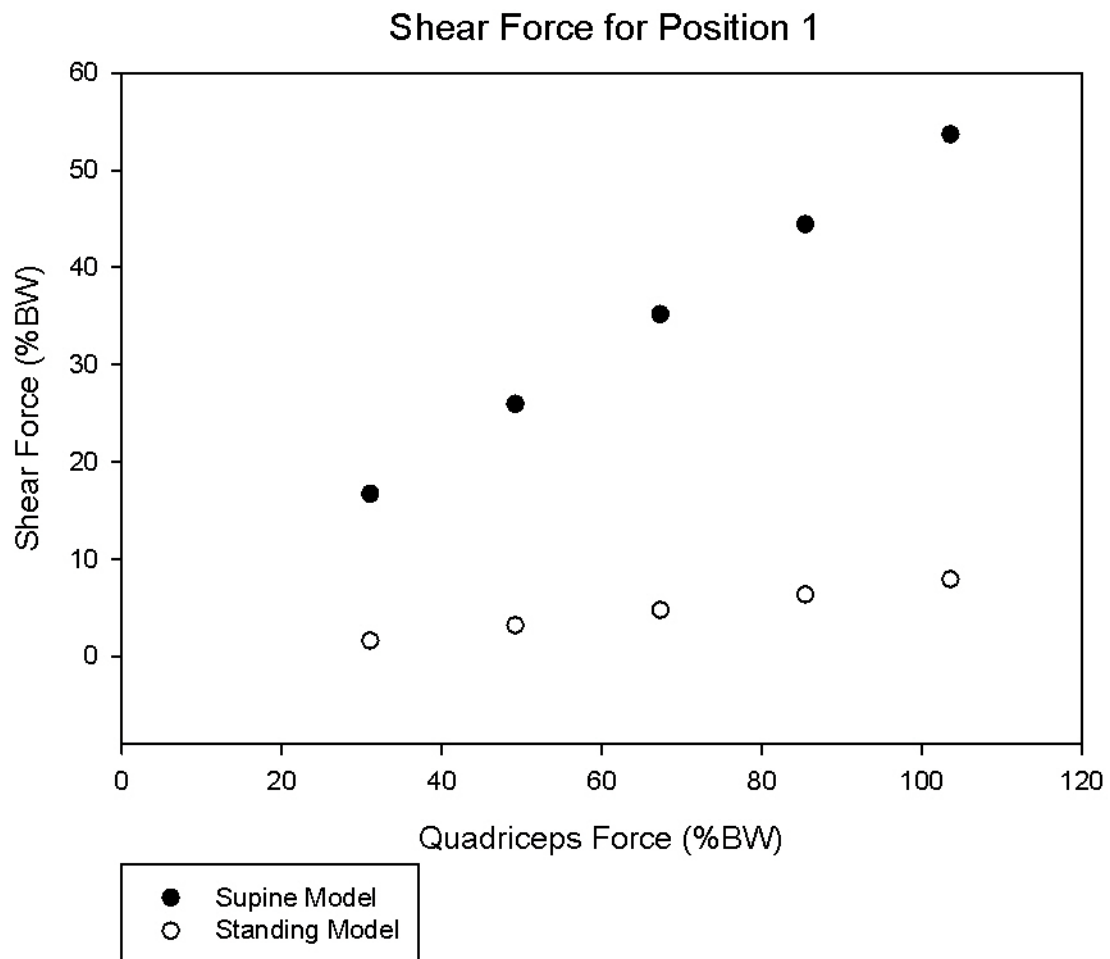


Figure 24. A representative example of the shear forces at position 1 for the supine and standing model as a percent of body weight (%BW) plotted against quadriceps muscle force.

Stimulus Condition	Fquad (%BW)	Fxhip (%BW)	Fyhip (%BW)	Fc (%BW)	Fv (%BW)
Tetanic	255	223	71.9	477	52.0
Doublet	28.7	9.72	52.1	38.3	12.5

Table 2. The solution to the five unknowns of the seated model for tetanic and doublet pulses are quadriceps force (Fquad), the horizontal force at the hip (Fxhip), the vertical force at the hip (Fyhip), compressive force at the distal femur (Fc), and shear force at the distal femur (Fv) and are reported in terms of percent body weight.

CHAPTER 5 DISCUSSION

The purposes of this study were: 1) to create two-dimensional, static models of the lower extremity in the supine position and the seated position, 2) to estimate the compressive and shear forces at the distal femur for both positions during FES, 3) to compare the internal compressive and shear forces generated at the distal femur from the standing model with those in the supine model, 4) to compare the compressive and shear forces at the distal femur of the seated model during tetanic and doublet quadriceps muscle contraction, and 5) to validate the supine model. Schematic free body diagrams were created to model the lower extremity for the supine and seated positions. Three, independent equilibrium equations were created for each of the two-dimensional, static models and two additional equations were obtained from the cut distal femur. By solving this system of equations, the compressive and shear forces at the distal femur for each of the conditions were determined. The primary findings of the study which supported both of the hypotheses are 1) the standing model estimated more compressive force and less shear force compared to the supine model, and 2) the tetanic quadriceps muscle contraction in the seated model resulted in higher estimated compressive and shear forces compared to the doublet quadriceps muscle contraction. Also, the validation testing revealed that only 3.4% error occurred between the force predicted by the supine model and the force measure for the tibial restraint. This low percent error could be interpreted as the supine model at least accurately predicting the external force at the tibial restraint.

There is much debate in the field of exercise science surrounding the most effective method of mechanically loading bone: muscle or gravity [51-54]. Frost's mechanostat theory supports that the greatest mechanical loading of bone is predominately due to muscle forces [22, 55]. However, after periods of extended bed rest [56] or space flight [57, 58] there is a significant decrease in BMD due to a loss of gravitational load. It is difficult and unnecessary to separate these mechanical loading mechanisms because a combination of both should yield

greatest preservation of BMD. Nevertheless, SCI individuals offer a unique opportunity to examine the musculoskeletal effects of a loss of muscle and gravitational loading and the effects of interventions which strive to reproduce muscle contraction, gravitational loading, or a combination of these. A longitudinal study of a standing exercise paradigm is currently ongoing and preliminary findings suggest that the femur of the limb which receives quadriceps muscle stimulation in combination with standing has higher BMD compared the opposite femur that only experiences the gravitational loading of standing. These results are very powerful because the opposite femur serves as the within subject control for age, sex, genetic pool, and hormonal status. It can be surmised that the greatest stimuli for bone is a combination of mechanical loading from muscle and gravity.

While the supine model predicts compressive forces that reach approximately 191% of body weight which could potentially prevent bone loss [37], it unfortunately is accompanied by a shear force that reaches approximately 62% of body weight. The standing model estimates the maximum compressive and shear forces at the distal femur to be 240% and 24% of body weight, respectively. Standing in combination with FES offers a safe and effective way to prevent BMD loss following a spinal cord injury especially when compared to the supine model. Because the standing model is an example of a closed-kinetic-chain exercise and the supine model is an open-kinetic-chain exercise this comparison can also provide insight into non-SCI exercises. Following an anterior cruciate ligament (ACL) reconstruction surgery, many rehabilitation specialists have advocated against open-kinetic-chain exercises because of high shear forces at the knee [42, 59-61]. The present study demonstrated that when quadriceps muscle force remains uniform across models, the supine model produces more shear force than the standing model which is consistent with ACL literature.

A similar study created a two-dimensional model to compare the tibiofemoral joint forces during open kinetic-chain-exercises and closed-kinetic-chain exercises [62]. They found that closed-kinetic-chain exercises have significantly more compressive forces

compared to open-kinetic-chain exercises when the lower extremity was at the same position, attributing this to more axial loading [62]. Closed-kinetic-chain exercises include body weight which results in more compressive forces and stability at the joint while limiting shear forces [60, 63]. Shear forces of 20% of body weight and 43% of body weight have been reported for isometric, weight bearing and isometric, non-weight bearing exercises, respectively [42, 64]. These previous studies support the findings of the present study and help to explain why the standing model has more compressive force and less shear force than the supine model for the same limb position.

Many studies have explored the biomechanics of the knee and the effects of changing the knee angle. It is well-documented that the highest shear forces occur at 90° of knee flexion during open-kinetic chain exercises [42, 45, 62]. A 90° knee flexion angle is also the angle of the reported femoral fracture of the individual with SCI during an FES protocol [41]. Although potentially harmful forces can be generated during this angle of knee flexion, it is still used to determine muscle physiology for SCI individuals [65-68]. The quadriceps muscle is at its optimal length at 90-100° of knee flexion [43] and isometric training at this position results in increasing isometric knee extension torque throughout the range of motion [10]. The equations of the seated model, from the present study, calculated the quadriceps muscle force and the compressive and shear forces at the distal femur during FES of the quadriceps muscle. When a tetanic quadriceps train was modeled, dangerously large compressive and shear forces were estimated at the distal femur. However, the seated model with a doublet pulse estimated much lower compressive and shear forces. The doublet protocol can offer a safe alternative to determine muscle physiology compared to other types of electrical stimulation, while maintaining the desired 90° of knee flexion.

Limitations and Future Work

While these mathematical models produce valuable insight into potential forces at the distal femur during FES of the quadriceps muscle, they are not without limitations. First of

all, these models were derived to represent the SCI population but the anthropometric values were determined from a non-SCI cohort. Therefore, the models might not represent all individuals with SCI because of the musculoskeletal changes that occur following a spinal cord injury. The models also did not account for contracture or passive tension but attributed all force generated to the quadriceps muscle group.

The validation testing only examined one of the six positions so that muscle fatigue would not confound the results. Therefore, more data collection would be needed to determine if muscle fatigue would be an issue, to determine an ideal number of contractions at each position, and to determine if a different stimulus intensity would be more suitable. Also, only one subject was used for the validation testing so many subjects would be required to determine if the percent error would remain low with a larger cohort. Since the model is intended to reflect a SCI population, then the validation of the supine model needs to be tested on individuals with spinal cord injury.

Another drawback of the models is that they are not patient-specific. Future work could include computed tomography (CT) or magnetic resonance imaging (MRI) to obtain accurate body composition of the subject. These images could then be used to generate a finite element (FE) model. FE modeling would add another dimension to the current 2D model and could more accurately estimate the compressive and shear forces at the distal femur. However, imaging and FE modeling would be much more expensive and time-consuming. Also, the purpose of this study was to compare the 2D supine model to the previously created 2D standing model. Therefore, if a FE model were created for the supine position, one would also need to be created for the standing position to allow for a comparison.

Conclusions

When administering FES to a SCI population it is essential to understand the forces which are generated and their potentially harmful repercussions. The standing model

produced more compressive forces and less shear forces at the distal femur than the supine model incorporating the same joint positions. Since the standing model is a closed-kinetic-chain exercise, the knee has forces that are more axially oriented and therefore limit shear forces. According to the comparison of the standing and supine model, the standing model is superior and should not only affect BMD to a greater extent than the supine model but also is a safer training protocol for individuals with spinal cord injury.

The seated mathematical model produced valuable results which compared a tetanic train and a doublet pulse as types of FES. A tetanic train of the quadriceps muscles, large enough to fracture a femur, generated high compressive and shear forces compared to a doublet pulse, as hypothesized. Since a doublet pulse has been shown to be an effective way to measure muscle physiology at 90° of knee flexion, it should be used in place of tetanic trains for the SCI population.

REFERENCES

1. Field-Fote, E.C., *Spinal cord injury rehabilitation*. 2009, Philadelphia, PA: F. A. Davis. p.
2. Jacobs, P.L. and M.S. Nash, *Exercise recommendations for individuals with spinal cord injury*. *Sports Med*, 2004. **34**(11): p. 727-51.
3. *International Standards for Neurological Classification of SCI*. 2002, American Spinal Injury Association: Atlanta, Georgia.
4. Vestergaard, P., et al., *Fracture rates and risk factors for fractures in patients with spinal cord injury*. *Spinal Cord*, 1998. **36**(11): p. 790-6.
5. Lidal, I.B., et al., *Health-related quality of life in persons with long-standing spinal cord injury*. *Spinal Cord*, 2008. **46**(11): p. 710-5.
6. Lieber, R.L., *Skeletal muscle structure, function, & plasticity*. 2002, Baltimore, MD: Lippincott Williams & Wilkins.
7. Frotzler, A., et al., *Bone steady-state is established at reduced bone strength after spinal cord injury: a longitudinal study using peripheral quantitative computed tomography (pQCT)*. *Bone*, 2008. **43**(3): p. 549-55.
8. Eser, P., et al., *Relationship between the duration of paralysis and bone structure: a pQCT study of spinal cord injured individuals*. *Bone*, 2004. **34**(5): p. 869-80.
9. Comarr, A.E., R.H. Hutchinson, and E. Bors, *Extremity fractures of patients with spinal cord injuries*. *Am J Surg*, 1962. **103**: p. 732-9.
10. Bandy, W.D. and W.P. Hanten, *Changes in torque and electromyographic activity of the quadriceps femoris muscles following isometric training*. *Phys Ther*, 1993. **73**(7): p. 455-65; discussion 465-7.
11. Lieber, R.L., et al., *Long-term effects of spinal cord transection on fast and slow rat skeletal muscle. II. Morphometric properties*. *Experimental Neurology*, 1986. **91**(3): p. 435-48.
12. Giangregorio, L. and N. McCartney, *Bone loss and muscle atrophy in spinal cord injury: epidemiology, fracture prediction, and rehabilitation strategies*. *J Spinal Cord Med*, 2006. **29**(5): p. 489-500.
13. Biering-Sorensen, F., H. Bohr, and O. Schaadt, *Bone mineral content of the lumbar spine and lower extremities years after spinal cord lesion*. *Paraplegia*, 1988. **26**(5): p. 293-301.

14. Castro, M.J., et al., *Influence of complete spinal cord injury on skeletal muscle within 6 mo of injury*. J Appl Physiol, 1999. **86**(1): p. 350-8.
15. Burnham, R., et al., *Skeletal muscle fibre type transformation following spinal cord injury*. Spinal Cord, 1997. **35**(2): p. 86-91.
16. Gerrits, H.L., et al., *Contractile properties of the quadriceps muscle in individuals with spinal cord injury*. Muscle Nerve, 1999. **22**(9): p. 1249-56.
17. Biering-Sorensen, B., et al., *Muscle after spinal cord injury*. Muscle Nerve, 2009. **40**(4): p. 499-519.
18. Wilmet, E., et al., *Longitudinal study of the bone mineral content and of soft tissue composition after spinal cord section*. Paraplegia, 1995. **33**(11): p. 674-7.
19. Shields, R.K., et al., *Peripheral quantitative computed tomography: measurement sensitivity in persons with and without spinal cord injury*. Arch Phys Med Rehabil, 2006. **87**(10): p. 1376-81.
20. Dudley-Javoroski, S. and R.K. Shields, *Muscle and bone plasticity after spinal cord injury: review of adaptations to disuse and to electrical muscle stimulation*. J Rehabil Res Dev, 2008. **45**(2): p. 283-96.
21. Mueller, M.J. and K.S. Maluf, *Tissue adaptation to physical stress: a proposed "Physical Stress Theory" to guide physical therapist practice, education, and research*. Phys Ther, 2002. **82**(4): p. 383-403.
22. Frost, H.M., *Bone "mass" and the "mechanostat": a proposal*. Anat Rec, 1987. **219**(1): p. 1-9.
23. Klein-Nulend, J., R.G. Bacabac, and M.G. Mullender, *Mechanobiology of bone tissue*. Pathol Biol (Paris), 2005. **53**(10): p. 576-80.
24. Frost, H.M., *Vital biomechanics: proposed general concepts for skeletal adaptations to mechanical usage*. Calcif Tissue Int, 1988. **42**(3): p. 145-56.
25. Shields, R.K., S. Dudley-Javoroski, and L.A. Law, *Electrically induced muscle contractions influence bone density decline after spinal cord injury*. Spine (Phila Pa 1976), 2006. **31**(5): p. 548-53.
26. Shields, R.K. and S. Dudley-Javoroski, *Musculoskeletal adaptations in chronic spinal cord injury: effects of long-term soleus electrical stimulation training*. Neurorehabil Neural Repair, 2007. **21**(2): p. 169-79.
27. Baldi, J.C., et al., *Muscle atrophy is prevented in patients with acute spinal cord injury using functional electrical stimulation*. Spinal Cord, 1998. **36**(7): p. 463-9.

28. Martin, T.P., et al., *Influence of electrical stimulation on the morphological and metabolic properties of paralyzed muscle*. J Appl Physiol, 1992. **72**(4): p. 1401-6.
29. Gerrits, H.L., et al., *Effects of training on contractile properties of paralyzed quadriceps muscle*. Muscle Nerve, 2002. **25**(4): p. 559-67.
30. Gerrits, H.L., et al., *Variability in fibre properties in paralysed human quadriceps muscles and effects of training*. Pflugers Arch, 2003. **445**(6): p. 734-40.
31. Cramer, R.M., et al., *Effects of electrical stimulation-induced leg training on skeletal muscle adaptability in spinal cord injury*. Scand J Med Sci Sports, 2002. **12**(5): p. 316-22.
32. Cramer, R.M., et al., *Effects of electrical stimulation leg training during the acute phase of spinal cord injury: a pilot study*. Eur J Appl Physiol, 2000. **83**(4 -5): p. 409-15.
33. Hartkopp, A., et al., *Effect of training on contractile and metabolic properties of wrist extensors in spinal cord-injured individuals*. Muscle Nerve, 2003. **27**(1): p. 72-80.
34. Cramer, R.M., et al., *Effect of load during electrical stimulation training in spinal cord injury*. Muscle Nerve, 2004. **29**(1): p. 104-11.
35. Shields, R.K. and S. Dudley-Javoroski, *Musculoskeletal plasticity after acute spinal cord injury: effects of long-term neuromuscular electrical stimulation training*. J Neurophysiol, 2006. **95**(4): p. 2380-90.
36. Dudley-Javoroski, S. and R.K. Shields, *Dose estimation and surveillance of mechanical loading interventions for bone loss after spinal cord injury*. Phys Ther, 2008. **88**(3): p. 387-96.
37. Dudley-Javoroski, S. and R.K. Shields, *Asymmetric bone adaptations to soleus mechanical loading after spinal cord injury*. J Musculoskelet Neuronal Interact, 2008. **8**(3): p. 227-38.
38. Goktepe, A.S., et al., *Does standing protect bone density in patients with chronic spinal cord injury?* J Spinal Cord Med, 2008. **31**(2): p. 197-201.
39. Kunkel, C.F., et al., *Effect of "standing" on spasticity, contracture, and osteoporosis in paralyzed males*. Arch Phys Med Rehabil, 1993. **74**(1): p. 73-8.
40. Frey Law, L.A. and R.K. Shields, *Femoral loads during passive, active, and active-resistive stance after spinal cord injury: a mathematical model*. Clin Biomech (Bristol, Avon), 2004. **19**(3): p. 313-21.

41. Hartkopp, A., et al., *Bone fracture during electrical stimulation of the quadriceps in a spinal cord injured subject*. Archives of Physical Medicine & Rehabilitation, 1998. **79**(9): p. 1133-6.
42. Smidt, G.L., *Biomechanical analysis of knee flexion and extension*. J Biomech, 1973. **6**(1): p. 79-92.
43. Dudley-Javoroski, S., et al., *Doublet stimulation protocol to minimize musculoskeletal stress during paralyzed quadriceps muscle testing*. J Appl Physiol, 2008. **104**(6): p. 1574-82.
44. Ahmed, A.M., D.L. Burke, and A. Hyder, *Force analysis of the patellar mechanism*. J Orthop Res, 1987. **5**(1): p. 69-85.
45. Mesfar, W. and A. Shirazi-Adl, *Biomechanics of the knee joint in flexion under various quadriceps forces*. Knee, 2005. **12**(6): p. 424-34.
46. Singerman, R., J. Berilla, and D.T. Davy, *Direct in vitro determination of the patellofemoral contact force for normal knees*. J Biomech Eng, 1995. **117**(1): p. 8-14.
47. Chaffin, D.B., Andersson, Gunnar B.J., Martin, Bernard, Martin J., *Occupational Biomechanics*. Third ed. 1999: Wiley-Interscience.
48. Dahlkvist, N.J., P. Mayo, and B.B. Seedhom, *Forces during squatting and rising from a deep squat*. Eng Med, 1982. **11**(2): p. 69-76.
49. Ellis, M.I., B.B. Seedhom, and V. Wright, *Forces in the knee joint whilst rising from a seated position*. J Biomed Eng, 1984. **6**(2): p. 113-20.
50. van Eijden, T.M., W. de Boer, and W.A. Weijs, *The orientation of the distal part of the quadriceps femoris muscle as a function of the knee flexion-extension angle*. J Biomech, 1985. **18**(10): p. 803-9.
51. Beck, B.R., *Muscle forces or gravity--what predominates mechanical loading on bone? Introduction*. Med Sci Sports Exerc, 2009. **41**(11): p. 2033-6.
52. Robling, A.G., *Is bone's response to mechanical signals dominated by muscle forces?* Med Sci Sports Exerc, 2009. **41**(11): p. 2044-9.
53. Kohrt, W.M., D.W. Barry, and R.S. Schwartz, *Muscle forces or gravity: what predominates mechanical loading on bone?* Med Sci Sports Exerc, 2009. **41**(11): p. 2050-5.
54. Judex, S. and K.J. Carlson, *Is bone's response to mechanical signals dominated by gravitational loading?* Med Sci Sports Exerc, 2009. **41**(11): p. 2037-43.

55. Frost, H.M., *The mechanostat: a proposed pathogenic mechanism of osteoporoses and the bone mass effects of mechanical and nonmechanical agents*. Bone Miner, 1987. **2**(2): p. 73-85.
56. Leblanc, A.D., et al., *Bone mineral loss and recovery after 17 weeks of bed rest*. J Bone Miner Res, 1990. **5**(8): p. 843-50.
57. LeBlanc, A.D., et al., *Skeletal responses to space flight and the bed rest analog: a review*. J Musculoskelet Neuronal Interact, 2007. **7**(1): p. 33-47.
58. LeBlanc, A., et al., *Bone mineral and lean tissue loss after long duration space flight*. J Musculoskelet Neuronal Interact, 2000. **1**(2): p. 157-60.
59. Grodski, M. and R. Marks, *Exercises following anterior cruciate ligament reconstructive surgery: biomechanical considerations and efficacy of current approaches*. Res Sports Med, 2008. **16**(2): p. 75-96.
60. Graham, V.L., G.M. Gehlsen, and J.A. Edwards, *Electromyographic Evaluation of Closed and Open Kinetic Chain Knee Rehabilitation Exercises*. J Athl Train, 1993. **28**(1): p. 23-30.
61. Lindahl, O., A. Movin, and I. Ringqvist, *Knee extension. Measurement of the isometric force in different positions of the knee-joint*. Acta Orthop Scand, 1969. **40**(1): p. 79-85.
62. Lutz, G.E., et al., *Comparison of tibiofemoral joint forces during open-kinetic-chain and closed-kinetic-chain exercises*. J Bone Joint Surg Am, 1993. **75**(5): p. 732-9.
63. Shelbourne, K.D. and P. Nitz, *Accelerated rehabilitation after anterior cruciate ligament reconstruction*. Am J Sports Med, 1990. **18**(3): p. 292-9.
64. Morrison, J.B., *Function of the knee joint in various activities*. Biomed Eng, 1969. **4**(12): p. 573-80.
65. Kern, H., et al., *One year of home-based daily FES in complete lower motor neuron paraplegia: recovery of tetanic contractility drives the structural improvements of denervated muscle*. Neurol Res. **32**(1): p. 5-12.
66. Kern, H., et al., *Home-Based Functional Electrical Stimulation Rescues Permanently Denervated Muscles in Paraplegic Patients With Complete Lower Motor Neuron Lesion*. Neurorehabil Neural Repair.
67. Duffell, L.D., et al., *Long-term intensive electrically stimulated cycling by spinal cord-injured people: effect on muscle properties and their relation to power output*. Muscle Nerve, 2008. **38**(4): p. 1304-11.

68. Szecsi, J., et al., *A comparison of functional electrical and magnetic stimulation for propelled cycling of paretic patients*. Arch Phys Med Rehabil, 2009. **90**(4): p. 564-70.

APPENDIX A MODEL PARAMETERS

height=1.73 m

mass=68.04 kg

Anthrometric Data (Chaffin and Andersen)

Segment Lengths

Length of thigh = 24.5% of height

Length of shank = 24.6% of height

Length of foot = 3.9% of height

Center of mass (COM) of the thigh and shank from the knee

COM of the thigh = 56.7% of thigh length

COM of the shank = 43.3% of shank length

Limb weights

Weight of the head, arms and trunk = 67.55% of mass

Weight of the thigh = 9.87% of mass

Weight of the shank = 4.58% of mass

Weight of the foot = 1.42% of mass

APPENDIX B MATLAB CODE FOR THE SUPINE MODEL

```

% Other Supine Model which matches the quadriceps force of the standing
model
%Created by: Colleen McHenry
%Created on: April 16, 2010
%Last Modified on: May 28, 2010

format short

%Model height in meters
H=1.73;

%Model mass(weight) in kilograms
BW=68.04;

%Anthropometric Data
  %Leg lengths as a percentage of height
  Lth=0.245*H;
  Lsh=0.246*H;
  Lft=0.039*H;

  %Length to transducer from the knee
  Lm=0.400;

  %Center of mass of the thigh and the shank from the knee
  CMth=0.567*Lth;
  CMsh=0.433*Lsh;

  %Limb weights as a percentage of body weight
  Wth=0.0987*BW;
  Wsh=0.0458*BW;
  Wft=0.0142*BW;

%Quadriceps and Patellar Forces
[Fpat]=[25.3472 28.5481 32.3073 36.8873 42.7250 50.6058; 40.1205 45.2496
51.3664 58.9257 68.6828 81.994; 54.8939 61.9512 70.4255 80.9641 94.6406
113.3829; 69.6672 78.6527 89.4846 103.0025 120.5983 144.7715; 84.4406
95.3542 108.5438 125.0408 146.5561 176.1601];
[Fpat]=((Fpat*(1/100))*BW);
%disp([Fpat]);
[Fquad]=[31.0929 33.5603 36.6203 40.5365 45.7464 53.0354; 49.2151 53.1942
58.2238 64.7551 73.5398 85.9309; 67.3373 72.8280 79.8273 88.9737 101.3332
118.8265; 85.4595 92.4618 101.4308 113.1923 129.1266 151.7221; 103.5871
112.0956 123.0343 137.4109 156.9199 184.6176];
[Fquad]=((Fquad*(1/100))*BW);
%disp([Fquad]);

%Positions 1-6 and creating the corresponding angles
g=55;          %gamma(thigh angle measured from the thigh to the vertical)
a=75;          %alpha(shank angle measure from the shank to the vertical)
b=90-a;       %beta(angle of the force transducer)
c=a-5;
d=g-5;

```

```

f=5;          %Angle of quad to thigh

for i=1:1:5
    for k=1:1:6

        g=(g*pi)/180; %gamma converted to radians from degrees
        a=(a*pi)/180; %alpha converted to radians from degrees
        b=(b*pi)/180; %beta converted to radians
        c=(c*pi)/180;
        d=(d*pi)/180;
        f=(f*pi)/180;

        %From the Supine Model
        %Force at the Tibial Restraint
        Ra=((Wth*(Lth-
CMth)*sin(g))+(((Fquad(i,k)*cos(d))+Fpat(i,k)*cos(c))*(Lth*sin(g)))+(((
-1*Fquad(i,k)*sin(d))+Fpat*sin(c))*(Lth*cos(g)))+(Wsh*(Lth*sin(g)+CMsh*si
n(a)))+(Wft*((Lth*sin(g))+Lsh*sin(a))+Lft)))/(((cos(b))*((Lth*sin(g))+
Lm*sin(a))))-(sin(b)*((Lth*cos(g))+Lm*cos(a)))));

        %Horizontal Hip Joint Reaction Force
        Fxhip=((Fquad*sin(d))-Fpat*sin(c))-Ra(i,k)*sin(b));

        %Vertical Hip Joint Reaction Force
        Fyhip=((Wth)+(Fquad*cos(d))+Fpat*cos(c)+(Wsh)-
Ra(i,k)*cos(b))+Wft);

        %From the Cut Femur
        %Compressive Force

        Fc=((Fxhip(i,k)*sin(g))+Fyhip(i,k)*cos(g))+Fquad(i,k)*cos(f))-
(0.85*Wth*cos(g));

        %Shear Force
        Fv=((-
1*Fxhip(i,k)*cos(g))+Fyhip(i,k)*sin(g))+Fquad(i,k)*sin(f))-
(0.85*Wth*sin(g));

        %Display Solution
        Ra(i,k)=((Ra(i,k))/BW)*100;
        disp(Ra(i,k));

        Fxhip(i,k)=((Fxhip(i,k))/BW)*100;
        disp(Fxhip(i,k));

        Fyhip(i,k)=((Fyhip(i,k))/BW)*100;
        disp(Fyhip(i,k));

        Fc=(Fc/BW)*100;
        disp(Fc);

        Fv=(Fv/BW)*100;
        disp(Fv);

```

```
%Incrementing Angles
    g=((g*180)/pi)+4;
    a=((a*180)/pi)+2;
    b=((b*180)/pi)-2;
    c=((c*180)/pi)+2;
    d=((d*180)/pi)+4;
    f=((f*180)/pi);
end
g=55;
a=75;
b=15;
c=70;
d=50;
f=5;
end
```

APPENDIX C MATLAB CODE FOR THE SEATED MODEL

```

%Seated Model
%Created by: Colleen McHenry
%Created on: May 22, 2010
%Last Modified on: June 1, 2010

format short

%Model height in meters
H=1.73;
%H=1.93;

%Model mass(weight) in kilograms
BW=68.04;
%BW=70.45;

%Anthropometric Data
  %Leg lengths as a percentage of height
  Lth=0.245*H;
  Lsh=0.246*H;
  Lft=0.039*H;

  %Length to transducer from the knee
  Lm=0.451;
  %Lm=0.320;

  %Center of mass of the thigh and the shank from the knee
  CMth=0.567*Lth;
  CMsh=0.433*Lsh;

  %Limb weights as a percentage of body weight
  What=0.6755*BW;
  Wth=0.0987*BW;
  Wsh=0.0458*BW;
  Wft=0.0142*BW;

%Resistive Force
Ra=20.8;
%Ra=13.3;

%Angle from quad to thigh
f=5;
f=(f*pi)/180;

%From the Seated Model
  %Quadriceps Muscle Force
  Fquad=(((-Wth*(Lth-CMth))+(Ra*Lm)-((Wsh+Wft)*Lth))/(Lth*sin(f));
  disp(Fquad);

  %Horizontal Hip Joint Reaction Force
  Fxhip=((-Ra)+(Fquad*cos(f)));
  disp(Fxhip);

```

```
%Vertical Hip Joint Reaction Force
Fyhip=((0.5*What)+Wth+Wsh+Wft+(Fquad*sin(f)));
disp(Fyhip);

%From the Cut Femur
%Compressive Force
Fc=((Fquad*cos(f))+(Fxhip));
Fc=(Fc/BW)*100;
disp(Fc);

%Shear Force
Fv=(-0.5*What)+Fyhip-(0.85*Wth)+(Fquad*sin(f));
Fv=(Fv/BW)*100;
disp(Fv);
```